Review from Oyvind Breivik

First, the authors would like to sincerely thank the reviewers for their careful reading of the paper and their valuable comments to the manuscript and helpful suggestions. We further clarified several issues raised during the review process. Please find attached our revised paper and below a summary of how we responded to the comments. Our comments are reported in color in the text below.

General comments

- This paper describes a two-year experiment with a coupled WW3-NEMO setup. The experiment builds on earlier experiments by Breivik et al (2015) and others who investigated the impact of waves on the mixed layer. The paper is well written and clear.

- First, the change from a Dirichlet to a Neumann condition for the TKE flux should be discussed in more detail. It is not clear to me that comparing against an uncoupled run with a Dirichlet conditon is clean. A separate experiment should be run where the uncoupled model ingests a flux in the Neumann form, or alternatively a coupled run where the Dirichlet condition is used to communicate the TKE flux from WW3. That's a good point. From our point of view as soon as a coupling with a wave model is performed the surface boundary condition should systematically be in the Neumann (flux) form because the wave model naturally provides its information through a flux. In the uncoupled case, it is less clear what should be done. In Mellor and Blumberg (2004)[1] the authors consider both a Dirichlet condition (such that $e_{\rm sfc} = (15.8\alpha_{\rm CB})^{2/3} u_\star^2$ (their eq. (10))) and an equivalent Neumann condition ($K_e \partial_z e = 2\alpha_{\rm CB} u_\star^3$ (their eq. (3))) and they mention in their Sec. 7 that *"numerical solutions using Eqs. (1), (2), and "* a Dirichlet condition *"instead of"* a Neumann condition *"reproduced all of the calculations in Figs. 1, 3, and 4"*. Based on their finding, we preferred to focus our efforts in terms of additional simulations toward the clarification of the role of the Axell parameterization on our

[1] Mellor, G. and A. Blumberg, 2004: Wave Breaking and Ocean Surface Layer Thermal Response. J. Phys. Oceanogr., 34, 693698.

numerical results. But this would definitely be worth the effort to redo the Mellor & Blumberg experiment with NEMO to check if solutions are indeed insensitive to the nature of the TKE surface boundary condition in uncoupled cases. It should be emphasized that a Neumann (flux) boundary condition for TKE has been used earlier in various studies of wave-ocean coupling (e.g. Michaud et al., 2012) and is not something specific to our approach.

- The integration period is rather short. I think the authors should investigate whether there is sufficient convergence after just two years.
  We are not necessarily looking for convergence but we considered it was enough to illustrate the fact that our developments were actually producing the expected results. Integrating longer in time could also lead to drifts in the stratification independently from the wave effects and could thus distort our interpretation. We are lucid about the fact that we can not draw any conclusion on the long term impact of waves effect at global scales, a different experimental setup would be needed to do that.

- The Langmuir experiment is very interesting as it promises a way forward from the ETAU hack. I would like to see a quantification of how much changing from parameterized Stokes drift (1.6% of the wind speed) to a Stokes drift taken from WW3 gives you. I suspect the most important thing youve done is to change the factor from 0.15 to 0.30. Further on the Langmuir experiment, you dont seem to improve the Stokes drift discussion is interesting.
  Besides the calibration of the parameter c_{LC} we have also revised the way the input of Stokes drift contributing to Langmuir turbulence is computed. See in Fig. 1 at the end of this document the annual mean of the surface Stokes drift $\|\mathbf{u}^s(\eta)\|$ vs the surface Stokes drift as parameterized in the uncoupled case (i.e. $0.377\sqrt{\|\boldsymbol{\tau}\|/\rho_0}$). On average those two quantities are significantly different which partially explain the stronger role played by the LC parameterization in coupled simulations vs uncoupled ones.

- I suggest you read the appendix of Li et al (2017) where there is a description of the finite volume form of the profile by Breivik et al (2016).
  Thanks for pointing this out to us. We now make reference to App.

A of Li et al (2017) when introducing the finite-volume form of the Stokes drift profile. It seems that Wu et al. (2019) also considered such approach.

- Also, the recent paper by Wu et al (2019) discusses the combined impact (quite small!) of the Coriolis-Stokes force and the Stokes drift on tracer advection.
  We were aware of this paper but we forgot to mention it, it has been added to the revised manuscript. It is indeed well know that you should have both Stokes-Coriolis and the effect of Stokes drift on tracer/continuity equation all together otherwise it does not make any sense. Indeed, because of the geostrophic balance, the Stokes-Coriolis force must be counterbalanced by a pressure gradient which accounts for the Stokes drift. This combined impact seems indeed rather small also in our numerical experiments.

- Finally, a quantitative assessment of the relative impact of the various wave-induced processes is needed in order to give the reader an idea of their importance. This applies to the description in Sec 4.2.3 as mentioned below.
  In the revised manuscript an additional numerical experiment has been done to further assess the relative role of the different changes (see Tab. 2). This additional simulation allows to separate the impact of the modifications in the TKE scheme from the impact of the Langmuir cell parameterization. It suggests that for a 1/4° resolution the additional terms in the wave-averaged primitive equations have very small impact and that most of the improvements we see are related to the change in wind-stress, TKE closure and LC parameterization. We believe that Fig. 10 provides some hints on the relative role of each processes.

- Cost: You have run WW3 on half the resolution of NEMO at 20% added cost. Have you considered the added benefit of running the models on similar resolution? I presume this would cost more than twice the standalone NEMO run, so I sympathize with your decision, though.
  Considering a linear scaling going from 1/2° to 1/4° would increase the cost of the wave model by 8 and thus the added cost would be 160%. Besides the associated cost, our study was motivated by operational

purposes in the framework of CMEMS, that's the reason why we had to keep a reasonable added cost for the coupling with the waves.

- All told, I would say that after major revision (rerunning the experiments with Dirichlet or Neumann to make a clean comparison) and assessment of the relative importance of the wave-induced effects, this paper should be acceptable for publication in GMD.
  Our study provides in several ways a good starting to allow a clean separation between various effects. We could imagine refining it by implementing online diagnostics to assess the relative role of the different in the prognostic equation for TKE. This is however beyond the scope of this particular study and we think that a 1/4° resolution global oceanic configuration is probably not the adequate simulation to do that.
  Moreover, just like the example you give below for the combined impact of Stokes-Coriolis and the Stokes drift in tracer/mass equations the modifications we make are often not independent from each other and trying to test each modification individually may break some balances. We would have liked to prepare a figure showing the difference between $\Phi_{\rm oc}/\rho_0$ (the TKE flux from the wave model in the coupled case) vs $2\alpha_{\rm CB}u_\star^3$ (the TKE flux in the uncoupled case following Craig & Banner) because we did not have enough time to do so because additional experiments would have been needed ($\Phi_{\rm oc}$ was not stored in our standard outputs).

Detailed comments

- Fig 2 is a mess. Please explain in detail what is shown in the different panels and refer to those panels in the text. The figure headings are illegible. I am also surprised by the huge difference in average wave height and would like to see a more in-depth discussion of why this is so.
  Sorry for Fig. 2, the rendering of this figure is perfectly fine on a mac computer but there is something wrong on other operating systems. We have corrected this issue. On this figure we show the seasonal averaged of significant wave height as computed by WW3 on the left panels and the differences between the Charnock parameter computed by WW3 and the standard constant value. Such large deviations of

the Charnock parameters from the constant value 0.018 have also been observed for example by Pineau-Guillou et al. (2018) [2].

- 4.2.2 It is interesting that you have rewritten the Dirichlet conditon to a Neumann condition for the TKE flux. However, I think you should also investigate how this affects the results as you compare against an uncoupled run with a Dirichlet condition.
  Please see our comments on this aspect earlier in our reply.

- 4.2.3 The impact on MLD and SST does not separate between Langmuir, TKE flux, and stress. This needs to be done.
  As mentioned above, an additional numerical experiment has been done to separate those 3 effects and results are shown in Fig. 10.

- I was meant to say about the Langmuir mixing that you dont seem to improve the MLD much, but this is part of the general comment I was making that you need to separate the impact of the various processes.
  Based on the new version of Fig. 10, the effect of the parameterized Langmuir mixing is not significantly less than the effect of the revised TKE scheme. The Axell parameterization is necessary to make the MLD more consistent with observations.

[2] PineauGuillou, L., Ardhuin, F., Bouin, M.N., Redelsperger, J.L., Chapron, B., Bidlot, J.R. and Quilfen, Y. (2018), Strong winds in a coupled waveatmosphere model during a North Atlantic storm event: evaluation against observations. Q.J.R. Meteorol. Soc, 144 317-332

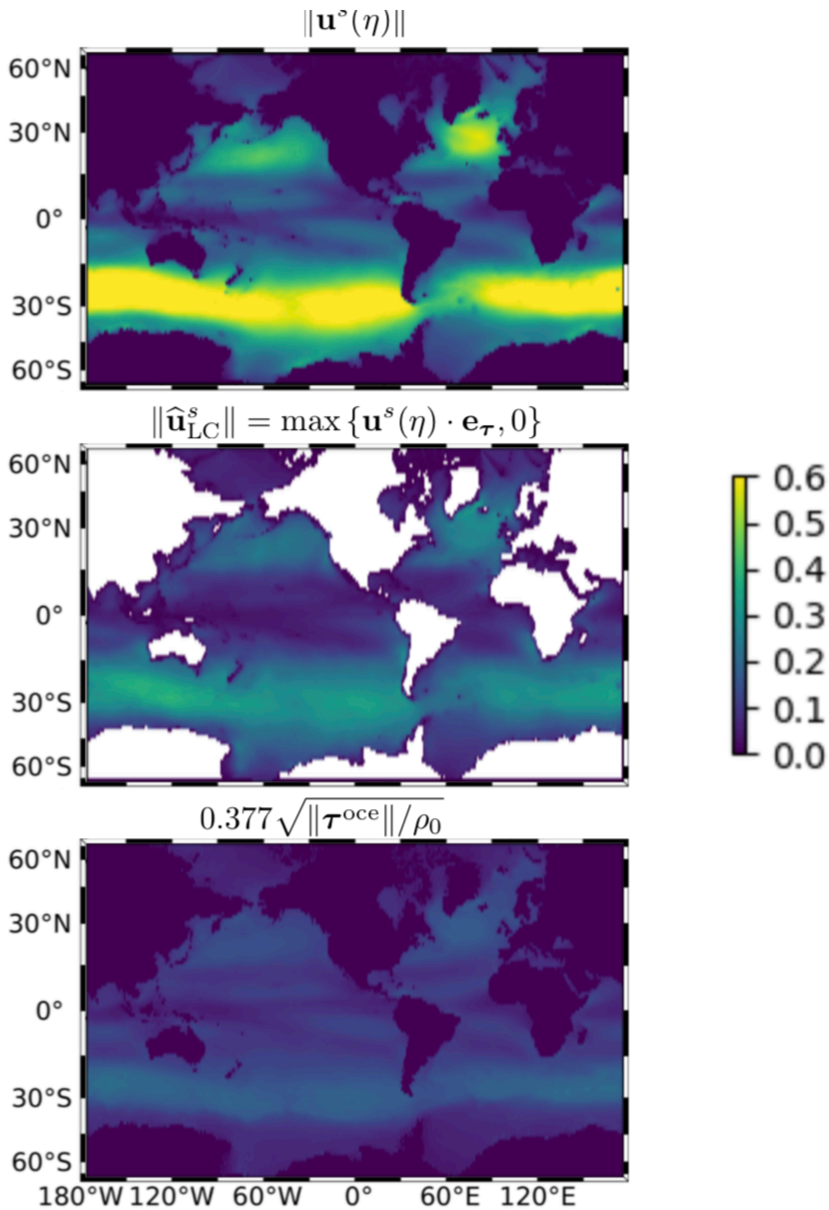

Figure 1: Annual average of surface Stokes drift module $\|\mathbf{u}^s(\eta)\|$ (top), of the portion of the Stokes drift aligned with the wind (middle), and of the surface Stokes drift as parameterized by $0.377\sqrt{\|\boldsymbol{\tau}^{\mathrm{oce}}\|/\rho_0}$ in the uncoupled case (bottom)

Review from George Nurser

First, the authors would like to sincerely thank the reviewers for their careful reading of the paper and their valuable comments to the manuscript and helpful suggestions. We further clarified several issues raised during the review process. Please find attached our revised paper and below a summary of how we responded to the comments. Our comments are reported in color in the text below.

Major Comments

- The authors have done a lot of work here in producing a coupled version of NEMO with WW3. The explanation of the extra terms added to NEMO is full, very much in the spirit of a GMD contribution, and it is good to see that the code is indeed publicly available.
  Thanks for this encouraging comment, the code is indeed publicly available and the developments are now in the process of being incorporated in the official NEMO release within the H2020 IMMERSE project.

- However, shortcuts have been taken e.g. the use of a neutral drag coefficient independent of Charnock number to estimate the atmospheric stress transferred into the waves, while the total atmospheric stress is separately calculated and depends on Charnock number and atmospheric stability.
  From your remark, it seems that our description of how the surface wind-stress is computed was not clear enough. The computation of the wind-stress in the wave model and in the oceanic model are both function of the Charnock parameter computed by the wave model. As mentionned in Sec. 3.2, in the wave model the general formula used is $\boldsymbol{\tau}_{\rm ww3} = \rho_a C_{\rm DN} \|\mathbf{u}_{10}^{\rm atm}\| \mathbf{u}_{10}^{\rm atm}$ where $C_{\rm DN} = \left(\frac{\kappa}{\ln\left(\frac{z}{z_0}\right)} \right)^2$ where z_0 depends on the Charnock parameter. The only difference between $\boldsymbol{\tau}_{\rm ww3}$ and the stress computed in the oceanic model is that the latter accounts for atmospheric stability. Note that what you call a "shortcut" is what is actually done in all coupled ocean-wave models as none of them guarantees energetic consistency (this point is often swept under the carpet in publications). Let us mention that :

  - Wave models in "forced mode" do not have any information on atmospheric temperature/humidity or SST which explains why they neglect atmospheric stability in the wind-stress computation.

  - The solution of wave models is very sensitive to wind-stress and our wave configuration has been designed and validated in forced mode with neutral drag coefficient. We tried to run WW3 with the same bulk formulation as NEMO but the quality of the wave solution was drastically deteriorated doing so.

We tried to further clarified those aspects in the revised manuscript.

- The testing of the modifications with 2-year runs is rather cursory, but I guess that the intention of that short testing period is more to check that the code is basically OK rather than to optimize the parameterizations. However, there really should be a test run that includes the changes to the TKE model coming from the flux condition using wave dissipation energy [(4) above] but not including the Langmuir cell parameterization.
Following your suggestion we have added a new case TKE_CPL in Tab. 2 which includes all ingredients but the Langmuir Cells parameterization. The results thus obtained are showed and discussed in Fig. 10 and Sec. 4.2.3.

- The paper generally seems a bit rushed, and the English while being perfectly readable, is not great; there are many extra ss where there should be none, etc.
Sorry for that, we tried to correct as much as possible these issues.

Detailed Comments

- p2,l39 Should refer to Lu et al. (2019).
We believe that instead of Lu et al. (2019) it should be Wu et al. (2019) ? A reference to Wu et al. (2019) has been added, in particular they also compute the Stokes drift as a "layer-averaged Stokes drift profile" based on the Breivik et al. (2016) profile. It is really not clear from their paper but it seems that they introduced in NEMO a Neumann (flux) boundary condition for the TKE equation. Thanks for pointing out this reference to us.

- p3,Eqs. (1)(4) Various w should be ω.
  It has been corrected in subgrid scale terms

- p3,Eqs.(1)(4) Please define p_h and p_s.
  Done

- p3,l78 τ^{oce} is not strictly the wind stress; it is that part of the stress that drives the ocean rather than developing the wave field.
  Indeed you are right, it has been changed.

- p3,l78 Please explain the dynamic boundary condition imposing the continuity of pressure at the air-sea interface
  We do not necessarily see what should be explained here. There must be no pressure jump at the air-sea interface, continuity of pressure translates into $p = p_{\text{atm}}$ at the interface with p_{atm} the atmospheric pressure at sea surface.

- p3,l80 $\omega(z = -H) = 0$. This is only true for terrain following coordinates, not for a generalized coordinate.
  Since ω is the dia-surface velocity component, at the lower boundary the no-normal flow boundary condition should read $\omega_{\text{bot}} = 0$ which is equivalent to $\mathbf{u} \cdot \mathbf{n} = 0$. We do not understand the issue here, the continuity equation equation integrates starting from $\omega = 0$ even with geopotential coordinate.

- p4,Eqs.(7)(8) Please define p^{J} and p^{FV}. I assume p^{J} is the J that is only significant in shallow water, defined in eq. (20) of Bennis et al., (2011). If so, then presumably p^{FV} represents the term $\frac{1}{2}\left[(\mathbf{u} + \mathbf{u}^s)^2 - \mathbf{u}^2\right]$ found e.g. on the RHS of Eq. (2) of Suzuki and Fox-Kemper (2016). This term would seem to scale with the vortex force term. Can the authors justify its neglect?
  Thanks for raising this issue. First we tried to clarify the notations in the paper and the way the additional wave related terms are introduced. In Suzuki and Fox-Kemper (2016) (SFK16) the Craik-Leibovich (CL) equations are used while our implementation relies on the more general wave-averaged primitive equations. In the CL equations the Bernoulli head term (let us note it $\mathcal{K}$) is defined as the kinetic energy increase due to the waves, i.e. $\mathcal{K} = \dfrac{\|\mathbf{u}^s + \mathbf{u}\|^2}{2} - \dfrac{\|\mathbf{u}\|^2}{2}$. In the wave-averaged equations, the form of the Bernoulli head is much more complicated

(see eq (9.20) in McWilliams et al. 2004 or the S^{Shear} term in Eq. (40) in Ardhuin et al. 2008) and it does not appear explicitly in our implementation because of the general weak vertical shears in the wave-mixed layer. The effect of that term was also found to be much weaker than S^J in shallow coastal environments, except in the surf zone. It is also mentioned in SFK16 (their Eq (14)) that the contribution of the Stokes shear force should be retained but since this term results from the combination of the vertical component of the vortex force with the Bernoulli head, it does not appear explicitly in our derivation. Finally, compared to the previous version of the manuscript, additional terms related to the slope of the vertical coordinate have been added in Eqs. (7) and (8). Those terms are pieces of the vortex force which need to be taken into account with a generalized vertical coordinate. They seldom appear in the literature because most people present the wave-averaged equations in geopotential coordinate.

- p4,Eq.(12) The wave pressure vector seems a little odd. It would be more natural to make $\mathcal{W}_{\text{prs}}$ the column vector of x- y- and vertical gradients, especially given that in p5, l118 you refer to the additional wave-induced barotropic forcing terms corresponding to the vertical integral of the ... $\mathcal{W}_{\text{prs}}$
  This has been reformulated by including the gradients in the $\mathcal{W}_{\text{prs}}$ term and removing the reference to the vertical integral of $\mathcal{W}_{\text{prs}}$ since after our simplifications this becomes a 2D horizontal field. The notations have been adapted and are now more consistent with Bennis et al. (2011) and Michaud et al. (2012) except that the S^J and S^{Shear} terms are expressed directly in terms of pressure terms $\widetilde{p}^J$ and $\widetilde{p}^{\text{Shear}}$.

- p5,Eq.(13) How do you decompose baroclinic and barotropic contributions to bottom drag when using non-linear bottom drag, as you do in these experiments (p13, l342) ?
  The non-linear bottom drag in the baroclinic mode is computed in an implicit way as $(C_D\|\mathbf{u}_h\|)^{n-1}\,\mathbf{u}_h^{n+1}$. Because of the linearization this term is analogous to a linear bottom drag and thus easy to separate into a barotropic and a baroclinic contributions. See Sec. 10.4 in the version 4.0 of the NEMO documentation for more details.

- p6,Figure1 You seem to have evaluated the primitive $\mathcal{I}_{\text{B14}}$,as you plot it out here. Why is it not written out explicitly like $\mathcal{I}_{\text{B16}}$, which is set

out at the bottom of p5?
The primitive of $\mathcal{S}_{\rm B14}$ requires the evaluation of the exponential integral function $\mathrm{Ei}(z)$. This special function is not available in the fortran standard while the erfc function in the primitive of $\mathcal{S}_{\rm B16}$ has an intrinsic procedure to compute it. This is the reason why we say that "The $\mathcal{S}_{\rm B16}$ is more adapted" for a Finite-Volume interpretation of the Stokes drift velocity.

- p6,l140141 This is a nice point. But note on l141 that summed to ω should summed with ω. More importantly, please briefly explain how $\omega+\omega^s$ is set; Eq. (10) looks more like a prognostic equation for e3 than a diagnostic equation for $\omega+\omega^s$.
We changed the wording. For your second remark, the overwhelming majority of NEMO simulations are done with a quasi-Eulerian vertical coordinate (either $z^\star$ or σ or a mixture of both) meaning that $\partial_t \mathrm{e}_3$ is given by the free-surface evolution (i.e. the coordinate system breathes with the free-surface) and in this context Eq. (10) is used to diagnose $\omega+\omega^s$. With a $\widetilde{z}$-coordinate $\partial_t \mathrm{e}_3$ is also prescribed by the evolution of the free-surface but also by the time-evolution of the coordinate surfaces but the rationale is the same: Eq. (10) is used to diagnose $\omega+\omega^s$. A sentence has been added to clarify this point.

- p9,l211 Should be $\|\mathbf{u}^s_{\rm LC}\| \propto \sqrt{\|\boldsymbol{\tau}\|}$
Yes, it is indeed the case, we agree it should be $\sqrt{\|\boldsymbol{\tau}\|}$

- p11,l27273 most of the momentum flux going into the waves is quickly transferred to the water column through wave breaking “we call this fraction $\boldsymbol{\tau}^{\rm oce}$. Do you mean $\boldsymbol{\tau}^{\rm oce}_{\rm WW3}$?
At this point, the notation $\boldsymbol{\tau}^{\rm oce}$ refers to the momentum flux used as a boundary condition for the oceanic model independently from the way it is computed. In practice it is indeed in the wave model that $\boldsymbol{\tau}^{\rm oce}$ is explicitly computed while in the oceanic model it is only diagnosed via equation (22). We hope this aspect is more clear in the revised manuscript.

- p11,l276 The Charnock number is used to give the surface roughness that presumably in fact allows wind to drive waves. Why is the WW3 model then not forced by a drag coefficient that includes this

effect? Also, why is the stress that drives the WW3 waves not stability-dependent?
This issue has been tackled earlier. The WW3 model is forced by a neutral drag coefficient which depends on the Charnock parameter. Historically, the stress computation in WW3 does not depend on atmospheric stability because only winds were provided to the wave model. As mentioned earlier, we tried to include the NEMO bulk formulation in WW3 but the wave solution thus obtained was extremely different from the original solution in the neutral case. Changing the bulk formulation requires a complete re-calibration of the wave model parameters. Again, to our knowledge our practice is customary to all coupled ocean-wave models.

- p11,Eq. (21) This equation does seem to ensure that momentum is conserved, although I guess $\boldsymbol{\tau}^{\text{atm}} - \boldsymbol{\tau}^{\text{atm}}_{\text{WW3}}$ may be much bigger than it should be.
Indeed momentum is not conserved because we compute twice the atmospheric flux with two different bulk formulations. As mentioned above, to our knowledge no coupled atmosphere-wave-ocean coupled model guarantees the momentum consistency (on top of the fact that most coupled models use a non-conservative grid-to-grid remapping of the wind-stress). This issue was already explicitly mentioned in the paper in Sec. 3.2: "*This strategy is not fully satisfactory since it breaks the momentum conservation*".

- p11,l289291 I understood that the situation is not that clear, especially for eddy resolving models, and that some consideration does need to be paid to the ocean current when calculating wind stress. E.g. the last sentence of Renault et al. (2018) states: A simulation without current feedbackby overestimating the eddy amplitude, lifetime, and spatial range.
We have to make a distinction depending on the type of coupling with the atmosphere. In a fully coupled mode, oceanic currents have to be taken into account because the corresponding loss of kinetic energy by the ocean is partially compensated by a re-energization of the ocean by the atmospheric PBL. In a forced mode, this re-energization is absent because atmospheric PBL processes are not accounted for and the loss of kinetic energy is thus largely overestimated. Since it is clear that in

a forced mode we don't represent the key feedback loops to properly represent the coupling between oceanic currents and the atmosphere we decided not to include this effect. But it should be clear that it is not a limitation of our implementation because it would be straightforward in coupled ocean-wave simulation to include the ocean current when computing the wind-stress (the namelist parameter rn_vfac just needs to be set to 1 instead of 0). The objective of our simulations is not to improve our physical understanding of ocean-wave processes but to check the robustness of our implementation.

- p13 Much of the first para seems to describe the wave model rather than its specific setup, so might fit in better into section 3.1.
The aspects of the wave model discussed in Sec. 4.1.1 are specific to our particular global configuration and other options are available in WW3. That's the reason why we structured it that way. From our point of view Sec. 3.1 should introduce things that are common to any WW3 simulation and necessary to understand where the coupling operates.

- p13,,l3378 The numerical options are the one commonly chosen by the Drakkar group. This is a bit confusing; please indicate which of the options described here are the Drakkar options, and whether there are other option choices described in the Drakkar website that are not described here.
In the manuscript we provide most of the information about the options used for the NEMO runs. For more details on those options, the namelist we used for the simulations are available under zenodo. In particular, see
https://zenodo.org/record/3331463/files/namelist˙cfg?download=1 and
https://zenodo.org/record/3331463/files/namelist˙ref?download=1
Furthermore as the reference to the Drakkar group was indeed confusing since Drakkar refers to NEMO global modelling community and not to specific numerical scheme, this sentence has been removed from the new manuscript

- p13,,l342 How does the lateral diffusivity vary away from the equator?
We have clarified it in the manuscript. The values of lateral (hyper)-viscosity and diffusivity we give in the paper are the values at the

equator. Away from the equator those values vary proportionally to Δx for the diffusivity and Δx^3 for the hyper-viscosity.

- p14,l348351 More specific details and/or references are required here. Is it only solar forcing that is given a diurnal cycle? A reference is required for the data correction to ensure consistency.
  This remark was indeed confusing and was simply wrong. The only correction we make to the forcing fields is to guarantee that their annual mean matches the annual mean obtained from satellites.

- p14,section4.1.3 There should be a test experiment with ST_CPL + changes to the TKE scheme but no Langmuir parameterization, to see whether the new TKE boundary condition makes any difference.
  This is a good point, we have done this additional experiment (referred to as TKE_CPL) and results are shown in Fig. 10. Note that besides the new boundary condition for TKE other changes have been done also to the boundary condition to diagnose the mixing length and an extra forcing term related to the Stokes drift shear has been added in the TKE equation.

- p14,section4.1.3 Please specify the initial conditions. Is it a spun up run of some standard NEMO setup? If so, give details.
  All ORCA025 experiments have been initialised from reanalysis GLORYS2V4 delivered by MERCATOR-OCEAN-INTERNATIONAL

- p15,Figure2 Various random missing letters on panel titles.
  Yes, the rendering of this figure was fine with Mac but is bad on other operating system. The problem has been solved.

- p16p17,section4.2.2 Given the amount of space devoted to the extra TKE injection (& 2 figures!), it really does seem strange that no run with ST˙CPL + changes to the TKE scheme but no Langmuir parameterization has been presented.
  A new simulation "TKE˙CPL" including all terms of the wave coupling except Langmuir parameterization has been performed and results where added in Figure 10, description on table 2 and discussion added in the text

- p17p19,section4.2.3 Give reference for ARGO MLD climatology, and specify the MLD criteria used in model and climatology.

ARGO data are issued from an updated version of de Boyer Montgut et al. (2004) where the criterion used is Rho_10m-Rho_10m*0,03. This has been added in the new manuscript

- p17p19,section4.2.3 Maps of discrepancies of MLD from ARGO, and zonal-average MLDs would be more convincing than the MLD pdfs.
  At first, we looked at maps of discrepancies, but due to the scarcity of the measurements the relevance of such comparison seems meaningless. From our point of view, the best way to compare is to co-localize the model results with the data. Eddies and fronts in the numerical simulations are not at the same place such that it makes more sense to look at PDFs rather than point-by-point differences. That is the reason why it has been chosen to use MLD pdfs. Although far from being an ideal diagnostic it at least shows a reliable statistical improvement of the MLDs when wave coupling is activated.

- p20,445 an increased heat content during winter leading to higher SST during summer. Is this the wrong way round?
  Indeed this the wrong way round, winter and summer have inverted in the new manuscript

- p29, appendixB It is not easy to see which of these solutions is best. On p9, l2516, you write Based on single-column experiments detailed in App. B, we find that parameter values in the range 0.15 - 0.3 provide satisfactory results compared to LES simulations Where are these LES simulation results?
  The LES results are the one presented in Noh et al. (2016) and our Figure B.1 should be compared to their Fig. 3. We modified the text to clarify this.

Development of a 2-way coupled ocean-wave model: assessment on a global NEMO(v3.6)-WW3(v6.02) coupled configuration

Xavier Couvelard[1], Florian Lemarié[2], Guillaume Samson[3], Jean-Luc Redelsperger[1], Fabrice Ardhuin[1], Rachid Benshila[4], and Gurvan Madec[5,2]

[1]Univ. Brest, CNRS, IRD, Ifremer, Laboratoire d'Océanographie Physique et Spatiale (LOPS), IUEM, Brest, France
[2]Univ. Grenoble Alpes, Inria, CNRS, Grenoble INP, LJK, 38000 Grenoble, France
[3]Mercator Océan, Toulouse, France
[4]LEGOS, University of Toulouse, CNES, CNRS, IRD, UPS, Toulouse, France
[5]Sorbonne Universités (UPMC, Univ Paris 06)-CNRS-IRD-MNHN, LOCEAN Laboratory, Paris, France

Correspondence: Florian Lemarié (florian.lemarie@inria.fr)

Abstract. This paper describes the implementation of a coupling between a three-dimensional ocean general circulation model (NEMO) and a wave model (WW3) to represent the interactions of the upper oceanic flow dynamics with surface waves. The focus is on the impact of such coupling on upper-ocean properties (temperature and currents) and mixed-layer ~~depths~~ depth (MLD) at global eddying scales. A generic coupling interface has been developed and the NEMO governing equations and boundary conditions have been adapted to include wave-induced terms following the approach of McWilliams et al. (2004) and Ardhuin et al. (2008). In particular, the contributions of Stokes-Coriolis, Vortex and surface pressure forces have been implemented on top of the necessary modifications of the tracer/continuity equation and turbulent closure scheme (a 1-equation TKE closure here). To assess the new developments, we perform a set of sensitivity experiments with a global oceanic configuration at $1/4^o$ resolution coupled with a wave model configured at $1/2^o$ resolution. Numerical simulations show a global increase of wind-stress due to the interaction with waves (via the Charnock coefficient) particularly at high latitudes, resulting in increased surface currents. The modifications brought to the TKE closure scheme and the inclusion of a parameterization for Langmuir turbulence lead to a significant increase of the mixing thus helping to deepen the MLD. This deepening is mainly located in the Southern Hemisphere and results in reduced sea-surface currents and temperatures.

1 Introduction

An accurate representation of ocean surface waves has long been recognized as essential for a wide range of applications ranging from marine meteorology to ocean and coastal engineering. Waves also play an important role in the short-term forecasting of extratropical and tropical cyclones by regulating sea-surface roughness (Janssen, 2008; Chen and Curnic, 2015; Hwang, 2015). More recently, the impact of waves on the oceanic circulation at global scale has triggered interest from the research and operational community (e.g. Hasselmann, 1991; Rascle and Ardhuin, 2009; D'Asaro et al., 2014; Fan and Griffies, 2014; Li et al., 2016; Law Chune and Aouf, 2018). In particular, surface waves are important for an accurate representation of air-sea interactions and their effect on fluxes of mass, momentum and energy through the wavy boundary layer must be taken into account in ocean-atmosphere coupled models. For example, the momentum flux through the air-sea interface has traditionally been parameterized using the near surface winds (typically at 10 meter) and the atmospheric surface layer stability (Fairall et al., 2003; Large and Yeager, 2009; Brodeau et al., 2016). The physics of the coupling depends on the kinematics and dynamics of the wave field. This includes a wide range of processes from wind-wave growth, nonlinear wave-wave ~~interactions~~interaction, wave-current ~~interactions~~ interaction to wave dissipation. Such complex processes can only be adequately represented by a wave model.

Besides affecting the air-sea fluxes, waves define the mixing in the oceanic surface boundary layer (OSBL) via breaking and Langmuir turbulence. For example, Belcher et al. (2012) showed that Langmuir turbulence should be important over wide areas of the global ocean and more particularly in the Southern ocean. In this region, they show that the inclusion of the effect of surface waves on the upper-ocean mixing during summertime allows for a reduction of systematic biases in the OSBL depth. Indeed their large eddy simulations (LES) suggest that under certain circumstances wave forcing can lead to large changes in the mixing profile throughout the OSBL and in the entrainment flux at the base of the OSBL. They concluded that wave forcing is always important when compared to buoyancy forcing, even in winter. Moreover, Polonichko (1997) and Van Roekel et al. (2012) emphasized the fact that the Langmuir cells intensity strongly depends on the alignment between the Stokes drift and wind direction. Langmuir turbulence is maximum when wind and waves are aligned and becomes weaker as the misalignment becomes larger. Li et al. (2017) highlighted that ignoring the alignment of wind and waves (i.e. assuming that wind and waves are systematically aligned) in the Langmuir cells parameterizations leads to excessive mixing particularly in winter.

Most previous studies of the impact of ocean-wave interactions at global scale have been using an offline one-way coupling and included only parts of the wave-induced terms in the oceanic model governing equations (e.g. Breivik et al., 2015; Law Chune and Aouf, 2018). In this study, the objective is to introduce a new online two-way coupled ocean wave modeling system with a great flexibility to be relevant for a large range of applications from climate modeling to regional short-term process studies. This modeling system is based on the Nucleus for European Modelling of the Ocean (NEMO, Madec, 2012) as the oceanic compartment and WAVEWATCH III® (hereinafter WW3, The WAVEWATCH III® Development Group, 2016) as the surface wave component. NEMO and WW3 are coupled using the OASIS Model Coupling Toolkit (OASIS3-MCT, Van Roekel et al., 2012; Craig et al., 2017) which is widely used in the climate and operational ~~communities~~community. The various steps for our implementation are the following (*i*) inclusion of all wave-induced terms in NEMO, only neglecting the terms relevant for the surf zone which is outside the scope here (*ii*) modification of the NEMO subgrid ~~scales~~ scale physics (including the bulk formulation) to include wave effects and a parameterization for Langmuir turbulence (*iii*) development of the OASIS interface within NEMO and WW3 for the exchange of data between ~~both~~ the models (*iv*) test of the implementation based on a realistic global configuration at $1/4^o$ for the ocean and $1/2^o$ for the waves.

To go into the details of those different steps, the paper is organized as follows. The modifications brought to the oceanic model primitive equations, their boundary conditions, and the subgrid ~~scales~~ scale physics to account for wave-ocean interactions are described in Sec. 2. This includes the addition of the Stokes-Coriolis force, the Vortex force, and the wave-induced pressure gradient. In Sec. 3 our modeling system coupling the NEMO oceanic model and the WW3 wave model via the OASIS3-MCT coupler is described in details. Numerical simulations are presented in Sec. 4 using a global configuration at

$1/4^o$ for the oceanic model and $1/2^o$ for the wave model. Using sensitivity runs, we assess those global configurations with particular emphasis on the impact of wave-ocean ~~interactions~~ interaction on mixed-layer depth, sea-surface temperature and currents, turbulent kinetic energy (TKE) injection, and kinetic energy. Finally, in Sec. 5, we summarize our findings and provide overall comments on the impact of two-way ocean-wave coupling in global configurations at eddy-permitting resolution.

2 Inclusion of wave-induced terms in the oceanic model NEMO

In order to set the necessary notations, we start by introducing the classical primitive equations solved by the NEMO ocean model. Note that between the two possible options to formulate the momentum equations, namely the so-called "vector invariant" and "flux" forms, we present here the first one which will be used for the numerical simulations in Sec. 4. With $\mathbf{u_h} = (u, v)$ the horizontal velocity vector, ω the dia-level velocity component, θ the potential temperature, ρ the density, ~~the~~ ζ the relative vorticity, p_h the hydrostatic pressure, p_s the surface pressure, the Reynolds-averaged equations (with $\langle\cdot\rangle$ the averaging operator, omitted here for simplicity) are

$$\partial_t u = +(f+\zeta)v - \frac{1}{2}\partial_x\|\mathbf{u_h}\|^2 - \frac{\omega}{\mathrm{e}_3}\partial_k u - \frac{1}{\rho_0}\left(\partial_x(p_s+p_h) - \frac{(\partial_k p_h)(\partial_x z)}{\mathrm{e}_3}(\partial_x z)\frac{(\partial_k p_h)}{\mathrm{e}_3}\right) - \frac{1}{\mathrm{e}_3}\partial_k\left\langle u' w\omega'\right\rangle + F^u \quad (1)$$

$$\partial_t v = -(f+\zeta)u - \frac{1}{2}\partial_y\|\mathbf{u_h}\|^2 - \frac{\omega}{\mathrm{e}_3}\partial_k v - \frac{1}{\rho_0}\left(\partial_y(p_s+p_h) - \frac{(\partial_k p_h)(\partial_y z)}{\mathrm{e}_3}(\partial_y z)\frac{(\partial_k p_h)}{\mathrm{e}_3}\right) - \frac{1}{\mathrm{e}_3}\partial_k\left\langle v' w\omega'\right\rangle + F^v \quad (2)$$

$$\partial_t(\mathrm{e}_3\theta) = -\partial_x(\mathrm{e}_3\theta u) - \partial_y(\mathrm{e}_3\theta v) - \partial_k(\theta\omega) - \frac{1}{\mathrm{e}_3}\partial_k\left\langle \theta' w\omega'\right\rangle + F^\theta \quad (3)$$

$$\partial_t \mathrm{e}_3 = -\partial_x(\mathrm{e}_3 u) - \partial_y(\mathrm{e}_3 v) - \partial_k\omega \quad (4)$$

$$\partial_k p = -\rho g \mathrm{e}_3 \quad (5)$$

Here k is a non-dimensional vertical coordinate, lateral derivatives ∂_x and ∂_y have to be considered along the model coordinate, and e_3 is the vertical scale factor given by $\mathrm{e}_3 = \partial_k z$, where z is the local depth and ρ is given by an equation of state (Roquet et al., 2015). The necessary boundary conditions include a kinematic surface and bottom boundary condition ~~for~~ which can be expressed in terms of the vertical velocity w

$$w(z=\eta) = \partial_t\eta + u|_{z=\eta}\,\partial_x\eta + v|_{z=\eta}\,\partial_y\eta + (E-P), \qquad w(z=-H) = -\,u|_{z=-H}\,\partial_x H - v|_{z=-H}\,\partial_y H \quad (6)$$

with η the height of the sea-surface and $(E-P)$ the mass flux across the sea-surface due to precipitations and evaporation, a momentum surface boundary condition for the Reynolds stress vertical terms

$$-\left\langle u' w\omega'\right\rangle\Big|_{z=\eta} = \frac{\tau_u^{\mathrm{oce}}}{\rho_0}, \qquad -\left\langle v' w\omega'\right\rangle\Big|_{z=\eta} = \frac{\tau_v^{\mathrm{oce}}}{\rho_0},$$

with $\boldsymbol{\tau}^{\mathrm{oce}} = (\tau_u^{\mathrm{oce}}, \tau_v^{\mathrm{oce}})$ ~~the wind stress vector, and the~~ a wind-stress vector which represents the part of the stress that drives the ocean, and a dynamic boundary condition ~~imposing the~~ on the free surface leading to the continuity of pressure ~~at~~ across the air-sea interface. The kinematic boundary conditions (6) for $w(z=\eta)$ and $w(z=-H)$ translate into ~~$w(z=\eta)=0$~~

$\omega(z=\eta)=(E-P)$ and $\omega(z=-H)=0$. We do not include explicitly here the boundary conditions for the tracer equations since they are unchanged from classical primitive equations models in the presence of wave motions. As mentioned earlier, in equations (1) to (5) prognostic variables have to be interpreted in an Eulerian-mean sense even if the averaging operator is not explicitly included.

2.1 Modification of governing equations and boundary conditions

Asymptotic expansions of the wave effects based on Eulerian velocities (McWilliams et al., 2004) or Lagrangian mean equations (Ardhuin et al., 2008) lead to the same self-consistent set of equations for weak vertical current shears. These are further applied and discussed by Uchiyama et al. (2010)~~and Bennis et al. (2011)~~, Bennis et al. (2011), Michaud et al. (2012), or Moghimi et al. (2013). The 3-component Stokes drift vector is $\mathbf{u}^s=(\widetilde{u}^s,\widetilde{v}^s,\widetilde{\omega}^s)$, and is non-divergent at lowest order (Ardhuin et al., 2008, 2017b). The coupled wave-current equations for the Eulerian mean velocity and tracers in a vector invariant form (the equivalent flux form is given in Appendix. A) are

$$\partial_t u = +(f+\zeta)(v+\widetilde{v}^s) - \frac{1}{2}\partial_x\|\mathbf{u_h}\|^2 - \frac{(\omega+\widetilde{\omega}^s)}{\mathrm{e}_3}\partial_k u - \frac{(\partial_x z)}{\mathrm{e}_3}\left(\widetilde{u}^s\partial_k u+\widetilde{v}^s\partial_k v\right) - \frac{\partial_x(p_s+\widetilde{p}^J)}{\rho_0}$$

$$- \frac{1}{\rho_0}\left(\partial_x(p_h+\widetilde{p}^{\mathrm{FV}\,\mathrm{Shear}}) - \frac{(\partial_k(p_h+\widetilde{p}^{\mathrm{FV}}))(\partial_x z)}{\mathrm{e}_3}(\partial_x z)\frac{\partial_k(p_h+\widetilde{p}^{\mathrm{Sh}}}{\mathrm{e}_3}\right.$$

$$\partial_t v = -(f+\zeta)(u+\widetilde{u}^s) - \frac{1}{2}\partial_y\|\mathbf{u_h}\|^2 - \frac{(\omega+\widetilde{\omega}^s)}{\mathrm{e}_3}\partial_k v - \frac{(\partial_y z)}{\mathrm{e}_3}\left(\widetilde{u}^s\partial_k u+\widetilde{v}^s\partial_k v\right) - \frac{\partial_y(p_s+\widetilde{p}^J)}{\rho_0}$$

$$- \frac{1}{\rho_0}\left(\partial_y(p_h+\widetilde{p}^{\mathrm{FV}\,\mathrm{Shear}}) - \frac{(\partial_k p_h+\widetilde{p}^{\mathrm{FV}}))(\partial_y z)}{\mathrm{e}_3}(\partial_y z)\frac{\partial_k(p_h+\widetilde{p}^{\mathrm{Shea}}}{\mathrm{e}_3}\right.$$

$$\partial_t(\mathrm{e}_3\theta) = -\partial_x(\mathrm{e}_3\theta(u+\widetilde{u}^s) - \partial_y(\mathrm{e}_3\theta(v+\widetilde{v}^s)) - \partial_k(\theta(\omega+\widetilde{\omega}^s)) - \frac{1}{\mathrm{e}_3}\partial_k\left\langle\theta' w\omega'\right\rangle + F^\theta$$

$$\partial_t \mathrm{e}_3 = -\partial_x(\mathrm{e}_3(u+\widetilde{u}^s)) - \partial_y(\mathrm{e}_3(v+\widetilde{v}^s)) - \partial_k(\omega+\widetilde{\omega}^s)$$

$$\partial_k\left(p_h+\widetilde{p}^{\mathrm{Shear}}\right) = -\rho g\mathrm{e}_3 - \partial_k{}^{\mathrm{FV}} + \rho_0\left(\widetilde{u}^s\partial_k u+\widetilde{v}^s\partial_k v\right)$$

where wave-induced terms are represented with tildes. The $\widetilde{F}^u$ and $\widetilde{F}^v$ terms represent the sink/source of wave-momentum due to breaking, bottom friction and wave-turbulence interaction. These terms will be neglected since they are expected to play a significant role only in the surf zone. The other extra contributions to the momentum equations include the Stokes-Coriolis force $\boldsymbol{\mathcal{W}}_{\mathrm{St-Cor}}$, the vortex force $\boldsymbol{\mathcal{W}}_{\mathrm{VF}}$, and a wave-induced pressure $\boldsymbol{\mathcal{W}}_{\mathrm{Prs}}$

$$\boldsymbol{\mathcal{W}}_{\mathrm{St-Cor}} = \begin{pmatrix} f\widetilde{v}^s \\ -f\widetilde{u}^s \\ 0 \end{pmatrix}, \quad \boldsymbol{\mathcal{W}}_{\mathrm{VF}} = \begin{pmatrix} \zeta\widetilde{v}^s - \frac{\widetilde{\omega}^s}{e_3}\partial_k u \\ -\zeta\widetilde{u}^s - \frac{\widetilde{\omega}^s}{e_3}\partial_k v \\ \frac{\widetilde{u}^s}{e_3}\partial_k u + \frac{\widetilde{v}^s}{e_3}\partial_k v \end{pmatrix}, \quad \boldsymbol{\mathcal{W}}_{\mathrm{Prs}} = \begin{pmatrix} \widetilde{p}^J+\widetilde{p}^{\mathrm{FV}} \\ \widetilde{p}^J+\widetilde{p}^{\mathrm{FV}} \\ \widetilde{p}^{\mathrm{FV}} \end{pmatrix}$$

$$\mathcal{W}_{\mathrm{St-Cor}} = \begin{pmatrix} f\widetilde{v}^s \\ -f\widetilde{u}^s \\ 0 \end{pmatrix}, \quad \mathcal{W}_{\mathrm{VF}} = \begin{pmatrix} \zeta\widetilde{v}^s - \frac{\widetilde{\omega}^s}{e_3}\partial_k u - \frac{(\partial_x z)}{e_3}\left(\widetilde{u}^s\partial_k u + \widetilde{v}^s\partial_k v\right) \\ -\zeta\widetilde{u}^s - \frac{\widetilde{\omega}^s}{e_3}\partial_k v - \frac{(\partial_y z)}{e_3}\left(\widetilde{u}^s\partial_k u + \widetilde{v}^s\partial_k v\right) \\ \frac{\widetilde{u}^s}{e_3}\partial_k u + \frac{\widetilde{v}^s}{e_3}\partial_k v \end{pmatrix},$$

$$\mathcal{W}_{\mathrm{Prs}} = -\frac{1}{\rho_0}\begin{pmatrix} \partial_x\left(\widetilde{p}^J + \widetilde{p}^{\mathrm{Shear}}\right) - (\partial_x z)\frac{\partial_k(\widetilde{p}^{\mathrm{Shear}})}{e_3} \\ \partial_y\left(\widetilde{p}^J + \widetilde{p}^{\mathrm{Shear}}\right) - (\partial_y z)\frac{\partial_k(\widetilde{p}^{\mathrm{Shear}})}{e_3} \\ \frac{1}{e_3}\partial_k\widetilde{p}^{\mathrm{Shear}} \end{pmatrix} \tag{12}$$

where the terms involving horizontal derivatives of ω have been neglected in $\mathcal{W}_{\mathrm{VF}}$. In $\mathcal{W}_{\mathrm{Prs}}$, the $\widetilde{p}^J$ term corresponds to a depth uniform wave-induced kinematic pressure term~~, while $\widetilde{p}^{\mathrm{FV}}$~~[1], while $\widetilde{p}^{\mathrm{Shear}}$ is a shear-induced three-dimensional pressure term[2] associated with the vertical component of the vortex force. The vortex force contribution $\mathcal{W}_{\mathrm{VF}}$ can be further simplified by neglecting the terms involving the vertical shear~~as in Bennis et al. (2011), thus leading to $\mathcal{W}_{\mathrm{VF}}\cdot(0,0,1)^t = 0$ and $\widetilde{p}^{\mathrm{FV}} = 0$~~. In particular, the vertical component of the vortex force is absorbed in a pressure term $\widetilde{p}^{\mathrm{Shear}}$ (that gives the S^{shear} term in the notations of A . That particular term was neglected in Bennis et al. (2011) because of the general weak vertical shears in the wave-mixed layer. The effect of that term was also found to be much weater than $\widetilde{p}^J$ in shallow coastal environments, except in the surf zone. This assumption has the advantage to leave the hydrostatic relation (11) unchanged. Our implementation of wave-induced terms in NEMO is inline with Bennis et al. (2011) and corresponds to the simplified form of (12)

$$\mathcal{W}_{\mathrm{St-Cor}} = \begin{pmatrix} f\widetilde{v}^s \\ -f\widetilde{u}^s \\ 0 \end{pmatrix}, \qquad \mathcal{W}_{\mathrm{VF}} = \begin{pmatrix} \zeta\widetilde{v}^s - \frac{\widetilde{\omega}^s}{e_3}\partial_k u \\ -\zeta\widetilde{u}^s - \frac{\widetilde{\omega}^s}{e_3}\partial_k v \\ 0 \end{pmatrix}, \qquad \mathcal{W}_{\mathrm{Prs}} = -\frac{1}{\rho_0}\begin{pmatrix} \partial_x\widetilde{p}^J \\ \partial_y\widetilde{p}^J \\ 0 \end{pmatrix}.$$

Because of geostrophy, it is obvious that the addition of the Stokes-Coriolis force requires the effect of the Stokes drift on the mass and tracers advection to be taken into account. Regarding the joint modification of the tracers and continuity equations, it is clear that constancy preservation is maintained (i.e. a constant tracer field should remain constant during the advective transport) and that an additional wave related forcing must be added to the barotropic mode. The NEMO barotropic mode has been modified accordingly since the surface kinematic boundary condition (6) in terms of vertical velocities w and associated $\widetilde{w}^s$ now reads

$$w + \widetilde{w}^s = \partial_t\eta + (u|_{z=\eta} + \widetilde{u}^s|_{z=\eta})\partial_x\eta + (v|_{z=\eta} + \widetilde{v}^s|_{z=\eta})\partial_y\eta + (E-P)$$

[1] In the notations of Ardhuin et al. (2008) this term corresponds to $\widetilde{p}^J = \rho_0 S^J$

[2] In the notations of Ardhuin et al. (2008) this term corresponds to $\widetilde{p}^{\mathrm{Shear}} = \rho_0 S^{\mathrm{Shear}}$

to express the fact that there is a source of mass at the surface that compensates the convergence of the Stokes drift, hence the barotropic mode is

$$\begin{cases} \partial_t \eta &= -\partial_x \left((H+\eta)(\overline{u} + \overline{\widetilde{u}}^s) \right) - \partial_y \left((H+\eta)(\overline{v} + \overline{\widetilde{v}}^s) \right) + P - E, \\ \partial_t \overline{u} &= +f\overline{v} - g\partial_x \eta - \dfrac{C_{b,x}}{(H+\eta)} \overline{u} + \overline{G^x} + \overline{\widetilde{G}^x} \\ \partial_t \overline{v} &= -f\overline{u} - g\partial_y \eta - \dfrac{C_{b,y}}{(H+\eta)} \overline{v} + \overline{G^y} + \overline{\widetilde{G}^y} \end{cases} \tag{13}$$

where $\overline{\phi} = \frac{1}{H+\eta}\int_{-H}^{\eta} \phi dz$, $\mathbf{C}_b = (C_{b,x}, C_{b,y})$ the bottom drag coefficients, $\mathbf{G} = (\overline{G^x}, \overline{G^x})$ is the usual NEMO forcing term containing coupling terms from the baroclinic mode as well as slowly varying barotropic terms (including nonlinear advective terms) held constant during the barotropic integration to gain efficiency. In (13), the $\overline{\widetilde{G}^x}$ and $\overline{\widetilde{G}^y}$ contain the additional wave-induced barotropic forcing terms corresponding to the vertical integral of the $\boldsymbol{\mathcal{W}}_{\rm St-Cor}$ ~~, $\boldsymbol{\mathcal{W}}_{\rm Prs}$,~~ and $\boldsymbol{\mathcal{W}}_{\rm VF}$ terms which are also held constant during the barotropic integration. A thorough analysis on the impact of the additional wave-induced terms on energy transfers within an oceanic model can be found in Suzuki and Fox-Kemper (2016). Note however that the study of Suzuki and Fox-Kemper (2016) is based on the Craik-Leibovich equations which are a special case of the more general wave-averaged primitive equations. Those sets of equations are equivalent to each other only up to first order in vertical shear.

2.2 Computation and discretization of Stokes drift velocity profile

Reconstructing the full Stokes drift ~~profiles~~ profile $\mathbf{u}^s(z)$ in the ocean circulation model would require obtaining the surface spectra of the Stokes drift from the wave model. Instead, profiles are generally reconstructed considering a few important parameters, including the Stokes drift surface value $\mathbf{u}_{\rm h}^{\mathbf{s}}(\eta)$ and the norm of the Stokes volume transport $\|\mathbf{T}^s\|$. In Breivik et al. (2014) and Breivik et al. (2016), Stokes drift velocity profiles are derived under the deep-water approximation in the general form $\mathbf{u}_{\rm h}^{\mathbf{s}}(z) = \mathbf{u}_{\rm h}^{\mathbf{s}}(\eta)\mathcal{S}(z,k_e)$ with k_e a depth-independent spatial wavenumber chosen such that the norm of the depth integrated Stokes transport (assuming an ocean of infinite depth) is equal to $\|\mathbf{T}^s\|$. The functions $\mathcal{S}_{\rm B14}(z,k_e)$ from Breivik et al. (2014) and $\mathcal{S}_{\rm B16}(z,k_e)$ from Breivik et al. (2016) for $z \in [-H,\eta]$ are given by

$$\mathcal{S}_{\rm B14}(z,k_e) = \left(\frac{e^{2k_e(z-\eta)}}{1-8k_e(z-\eta)} \right), \qquad \mathcal{S}_{\rm B16}(z,k_e) = e^{2k_e(z-\eta)} - \sqrt{2k_e\pi(\eta-z)}\,{\rm erfc}(\sqrt{2k_e(\eta-z)}).$$

with erfc the complementary error function. It can be easily shown that for an ocean of infinite depth, the vertical integral of those functions are respectively equal to $\frac{1}{6k_e}$ for $\mathcal{S}_{\rm B16}$ and $\frac{1.34089}{8k_e} \approx \frac{1}{5.97k_e}$ for $\mathcal{S}_{\rm B14}$. Standard computations of Stokes drift in numerical models are done in a finite difference sense, however due to the fast decay of $\mathbf{u}_{\rm h}^{\mathbf{s}}(z)$ with depth, a finite volume approach seems more adequate, in this case

$$(\mathbf{u}_{\rm h}^{\mathbf{s}})_k = \frac{\mathbf{u}_{\rm h}^{\mathbf{s}}(\eta)}{({\rm e}_3)_k} \int_{z_{k-1/2}}^{z_{k+1/2}} \mathcal{S}(z,k_e){\rm d}z = \frac{\mathbf{u}_{\rm h}^{\mathbf{s}}(\eta)}{({\rm e}_3)_k} \left[\mathcal{I}(z_{k+1/2},k_e) - \mathcal{I}(z_{k-1/2},k_e) \right]$$

Such finite-volume interpretation of the Stokes drift velocity can also be found in Li et al. (2017) and Wu et al. (2019). The $\mathcal{S}_{\rm B16}$ function is more adapted for this kind of approach since the primitive function does only require special functions

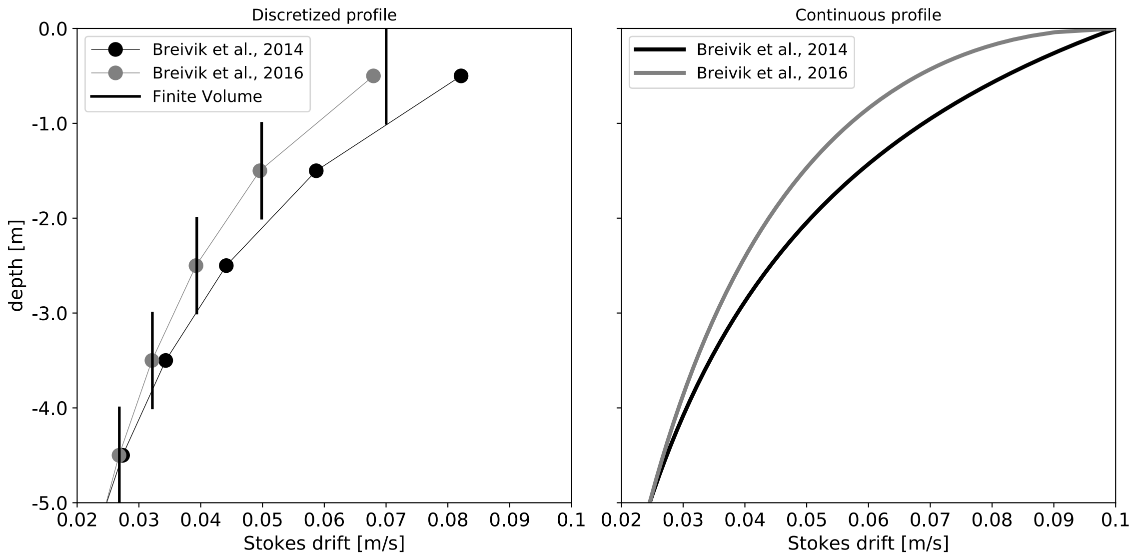

Figure 1. Left panel: reconstructed zonal component of Stokes drift profile for $\|\mathbf{T}^s\| = 0.4\,\mathrm{m}^2\,\mathrm{s}^{-1}$, $u^s(z=\eta) = 0.1\mathrm{m}\,\mathrm{s}^{-1}$, and $v^s(z=\eta) = 0\,\mathrm{m}\,\mathrm{s}^{-1}$ for a $1\,\mathrm{m}$ resolution vertical grid using the Breivik et al. (2014) function (black dots), Breivik et al. (2016) function (grey dots), and the finite volume Breivik et al. (2016) function (black vertical lines). Right panel: their continuous counterparts.

available in the fortran standard

$$\mathcal{I}_{\mathrm{B16}}(z,k_e) = \frac{1}{6k_e}\left[e^{2k_e(z-\eta)} + 4k_e(z-\eta)\mathcal{S}_{\mathrm{B16}}(z,k_e)\right]$$

Since NEMO is discretized on an Arakawa C-grid, the components of the Stokes drift velocity must be evaluated at cell interfaces, a simple average weighted by layer thicknesses is used :

$$\widetilde{u}^s_{i+1/2,j,k} = \frac{(\mathrm{e}_3)_{i,j,k}u^s_{i,j,k} + (\mathrm{e}_3)_{i+1,j,k}u^s_{i+1,j,k}}{2\,(\mathrm{e}_3)_{i+1/2,j,k}}, \qquad \widetilde{v}^s_{i,j+1/2,k} = \frac{(\mathrm{e}_3)_{i,j,k}v^s_{i,j,k} + (\mathrm{e}_3)_{i,j+1,k}v^s_{i+1,j,k}}{2\,(\mathrm{e}_3)_{i,j+1/2,k}}$$

Note that no explicit computation of the vertical component of the Stokes drift is necessary since in (7)-(11) $\widetilde{\omega}^s$ only appears summed ~~to~~ with ω such that the relevant variable is $\omega + \widetilde{\omega}^s$ as a whole. This quantity is diagnosed from the continuity equation (10) where the temporal evolution of vertical scale factors $\partial_t \mathrm{e}_3$ is given by the free-surface evolution when a quasi-Eulerian vertical coordinate is used (e.g. $z^\star$ or terrain-following coordinates).

As illustrated in Fig. 1, for the typical vertical resolution used in most global models the properties of the discretized Stokes profiles can be very different from their continuous counterparts. Indeed, the $\mathcal{S}_{\mathrm{B16}}(z,k_e)$ function has been considered superior to ~~the~~ $\mathcal{S}_{\mathrm{B14}}(z,k_e)$ because the vertical shear near the surface is expected to be better reproduced. However in Fig. 1 it is shown that this is no longer the case at a discrete level since the discrete vertical gradients at one meter depth turns out to be larger for $\mathcal{S}_{\mathrm{B14}}(z,k_e)$ compared to $\mathcal{S}_{\mathrm{B16}}(z,k_e)$. In this case, the fast variations of $\mathcal{S}_{\mathrm{B16}}(z,k_e)$ near the surface can not be represented by the computational vertical grid. A vertical resolution finer than the one currently used in most global ocean models near the surface would be required to properly represent the Stokes drift shear.

2.3 Subgrid ~~seales~~ scale physics

2.3.1 Turbulent kinetic energy prognostic equation and boundary conditions

Under the assumption of horizontal homogeneity, generally retained in general circulation models, the contribution from Stokes drift to the Turbulent Kinetic Energy (TKE) prognostic equation arises from the Vortex force vertical term $\mathcal{W}^z_{\rm VF} = \widetilde{u}^s \partial_z u + \widetilde{v}^s \partial_z v$ in the hydrostatic relation (11). Mimicking the way the TKE equation is usually derived (see e.g. Tennekes and Lumley, 1972) and using an averaging operator $\langle \cdot \rangle$ satisfying the "Reynolds properties", we find that the turbulent fluctuations, defined as $\phi' = \langle \phi \rangle - \phi$, $(\phi = p, \rho, u, v)$, associated with the $\mathcal{W}^z_{\rm VF}$ term are

$$(\mathcal{W}^z_{\rm VF})' = \widetilde{u}^s \partial_z u' + \widetilde{v}^s \partial_z v'$$

after multiplication by w' and averaging we obtain

$$\langle w' (\mathcal{W}^z_{\rm VF})' \rangle = \widetilde{u}^s \partial_z \langle u'w' \rangle + \widetilde{v}^s \partial_z \langle v'w' \rangle - \widetilde{u}^s \langle u' \partial_z w' \rangle - \widetilde{v}^s \langle v' \partial_z w' \rangle$$

where the last two terms in the right-hand-side cancel with similar terms appearing when forming the equations for $\langle u' \partial_t u' \rangle$ and $\langle v' \partial_t v' \rangle$ (see eqn (A.7) and (A.8) in Skyllingstad and Denbo (1995)). The extra terms associated with the Stokes drift in the horizontally homogeneous TKE equation are thus $u^s \partial_z \langle u'w' \rangle$ and $v^s \partial_z \langle v'w' \rangle$ which can be further rewritten as

$$\widetilde{u}^s \partial_z \langle u'w' \rangle = \langle u'w' \rangle \partial_z \widetilde{u}^s + \partial_z \left(\widetilde{u}^s \langle u'w' \rangle \right), \qquad \widetilde{v}^s \partial_z \langle v'w' \rangle = \langle v'w' \rangle \partial_z \widetilde{v}^s + \partial_z \left(\widetilde{v}^s \langle v'w' \rangle \right).$$

The first term will modify the shear production term, it can also be derived by taking the Lagrangian mean of the wave-resolved TKE equation (Ardhuin and Jenkins, 2006). The second will enter the TKE transport term which is usually parameterized as $-K_e \partial_z e$. The prognostic equation for the turbulent kinetic energy e in NEMO under the assumption that $K_e = A^{vm}$, with A^{vm} the eddy viscosity, is thus

$$\partial_t e = \frac{A^{vm}}{{\rm e}_3^2} \left[(\partial_k u)^2 + (\partial_k v)^2 + (\partial_k u)(\partial_k \widetilde{u}^s) + (\partial_k u^s v)(\partial_k \widetilde{v}^s) \right] - A^{vt} N^2 + \frac{1}{{\rm e}_3} \partial_k \left[\frac{A^{vm}}{{\rm e}_3} \partial_k e \right] - c_\epsilon \frac{e^{3/2}}{l_\varepsilon^2} \tag{14}$$

with A^{vt} the turbulent diffusivity, N the local Brunt-Väisälä Frequency, l_ε a dissipative length scale, and c_ε a constant parameter (generally such that $c_\varepsilon \approx 1/\sqrt{2}$). Once the value of e is know, eddy diffusivity/viscosity are given by

$$A^{vm} = C_m l_m \sqrt{e}, \qquad A^{vt} = A^{vm}/{\rm Prt}$$

with ${\rm Prt}$ the Prandtl number (see Sec. 10.1.3 in Madec (2012) for the detailed computation of ${\rm Prt}$), l_m a mixing length scale, and C_m a constant.

In addition to the modification of the shear production term in the TKE equation, the wave will affect the surface boundary condition both for e, l_m, and l_ε. The Dirichlet boundary condition traditionally used in NEMO for the TKE variable is modified into a Neumann boundary condition

$$\rho_0 \left(\frac{A^{vm}}{\mathrm{e}_3} \partial_k e \right)_{z=z_1} = -\rho_0 g \int_0^{2\pi} \int_0^{\infty} S_{\mathrm{ds}} d\omega d\theta = \Phi_{\mathrm{oce}} \tag{15}$$

meaning that the injection of TKE at the surface is given by the dissipation of the wave field via the wave-ocean S_{oce} term, which is a sink term in the wave model energy balance equation usually dominated by wave breaking, converted into an ocean turbulence source term. In practice, this sum of S_{ds} is obtained as a residual of the source term integration, hence it also includes unresolved fluxes of energy to the high frequency tail of the wave model. Due to the placement at cell interfaces of the TKE variable on the computational grid, the TKE flux is not applied at the free-surface but at the center of the top-most grid cell (i.e. at $z = z_1$). This amounts to interpret the half grid cell at the top as a constant flux layer which is consistent with the surface layer Monin-Obukhov theory.

The length scales l_m and l_ε are computed via two intermediate length scales l_{up} and l_{dwn} estimating respectively the maximum upward and downward displacement of a water parcel with a given initial kinetic energy. l_{up} and l_{dwn} are first initialized to the length scale proposed by Deardorff (1980), $l_{\mathrm{up}}(z) = l_{\mathrm{dwn}}(z) = \sqrt{2e(z)/N^2(z)}$. The resulting length scales are then limited not only by the distance to the surface and to the bottom but also by the distance to a strongly stratified portion of the water column such as the thermocline. This limitation amounts to control the vertical gradients of $l_{\mathrm{up}}(z)$ and $l_{\mathrm{dwn}}(z)$ such that they are not larger that the variations of depth (Madec, 2012)

$$\partial_k |l_.| \leq \mathrm{e}_3, \qquad l_. = l_{\mathrm{up}}, l_{\mathrm{dwn}}$$

Then the dissipative and mixing length scale are given by $l_m = \sqrt{l_{\mathrm{up}} l_{\mathrm{dwn}}}$ and $l_\varepsilon = \min(l_{\mathrm{up}}, l_{\mathrm{dwn}})$. Following Redelsperger et al. (2001) (their Sec. 4.2.3), a boundary condition consistent with the Monin-Obukhov similarity theory for the length scale l_{dwn} (while l_{up} necessitates only a bottom boundary condition) is

$$l_{\mathrm{dwn}}(z = \eta) = \kappa \frac{(C_m c_\varepsilon)^{1/4}}{C_m} z_0$$

with κ the von Karman constant and C_m, c_ε the constant parameters in the TKE closure. The surface roughness length z_0 can be directly estimated from the significant wave height provided by the wave model as $z_0 = 1.6 H_s$ (Rascle et al., 2008, their eqn (5)) which provides a proxy for the scale of the breaking waves. Note that in our study, no explicit parameterization of the mixing induced by near-inertial waves has been added (Rodgers et al., 2014). As highlighted by Breivik et al. (2015), without activating this *ad hoc* parameterization in the standard NEMO TKE scheme, the model does not mix deeply enough. They also speculated that this *ad hoc* mixing could mask effects of wave-related mixing processes such as Langmuir turbulence. For this reason, it is thus not used in the present simulations.

2.3.2 Langmuir turbulence parameterization

Langmuir mixing is parameterized following the approach of Axell (2002). This parameterization takes the form of an additional source term $P_{\rm LC}$ in the TKE equation (14). $P_{\rm LC}$ is defined as

$$P_{\rm LC} = \frac{w_{\rm LC}^3}{d_{\rm LC}}$$

where $w_{\rm LC}$ represents the vertical velocity profile associated with Langmuir cells and $d_{\rm LC}$ their expected depth. Following Axell (2002), $w_{\rm LC}$ and $d_{\rm LC}$ are given by

$$w_{\rm LC} = \begin{cases} c_{\rm LC} \|\widehat{\mathbf{u}}^s_{\rm LC}\| \sin\left(-\frac{\pi z}{d_{\rm LC}}\right), & \text{if } -z \le d_{\rm LC} \\ 0, & \text{otherwise} \end{cases}, \qquad -\int_{-d_{\rm LC}}^{\eta} N^2(z) z dz = \frac{\|\widehat{\mathbf{u}}^s_{\rm LC}\|^2}{2}$$

where $\|\widehat{\mathbf{u}}^s_{\rm LC}\|$ is the portion of the surface Stokes drift contributing to Langmuir cells intensity and $c_{\rm LC}$ a constant parameter. In the absence of information about the wave field it is generally assumed that $\|\widehat{\mathbf{u}}^s_{\rm LC}\| \propto \|\boldsymbol{\tau}\|$$\|\widehat{\mathbf{u}}^s_{\rm LC}\| \propto \sqrt{\|\boldsymbol{\tau}^{\rm oce}\|}$. As mentioned in the introduction, Polonichko (1997) and Van Roekel et al. (2012) showed that the intensity of Langmuir cells is largely influenced by the angle between the Stokes drift and the wind direction. To reflect this dependency we account for this angle in our definition of $\|\widehat{\mathbf{u}}^s_{\rm LC}\|$ via

$$\|\widehat{\mathbf{u}}^s_{\rm LC}\| = \max\left\{\mathbf{u}^s(\eta)\cdot\mathbf{e}_{\boldsymbol{\tau}}, 0\right\}$$

$$\|\widehat{\mathbf{u}}^s_{\rm LC}\| = \max\left\{\mathbf{u}^s(\eta)\cdot\mathbf{e}_{\boldsymbol{\tau}}, 0\right\} \qquad (16)$$

with $\mathbf{e}_{\boldsymbol{\tau}}$ the unit vector in the wind-stress direction. The difference between the surface Stokes drift $\|\mathbf{u}^s(\eta)\|$ and $\|\widehat{\mathbf{u}}^s_{\rm LC}\|$ given by (16) is shown in Fig. 2 and compared to the usual parameterization of $\|\mathbf{u}^s(\eta)\|$ as $0.377\sqrt{\|\boldsymbol{\tau}^{\rm oce}\|/\rho_0}$ in the uncoupled case (see Madec, 2012). The modulation of $\|\widehat{\mathbf{u}}^s_{\rm LC}\|$ depending on the wind-stress orientation significantly reduces the input of the surface Stokes drift contributing to Langmuir cells intensity especially in the Southern ocean while other regions are less affected. Finally, a value for the parameter $c_{\rm LC}$ must be chosen. Based on single-column experiments detailed in App. B, we find that parameter values in the range $0.15-0.3$ provide satisfactory results compared to LES simulations the LES simulations of Noh et al. (2016) and will be considered for the numerical experiments discussed later in Sec. 4.2.

While the The Axell (2002) parameterization was already implemented in NEMO but there are three majors major novelties in our implementation: *(i)* The online coupled strategy allows us to use the surface Stokes drift directly delivered by the wave model instead of the original value empirically estimated from the wind speed (e.g. 1.6% of the 10m wind) *(ii)* we only considered the component of the Stokes drift aligned with the wind and *(iii)* based on a series of single column simulations (see appendix B) the coefficients $c_{\rm LC}$ evaluated to 0.15 by Axell (2002) is set up to a 0.3 value. Those changes together with the new surface boundary condition for the TKE equation, lead to a deeper penetration of the TKE inside the mixed layer and, as shown in Sec. 4.2.3, greatly improved the MLD distribution.

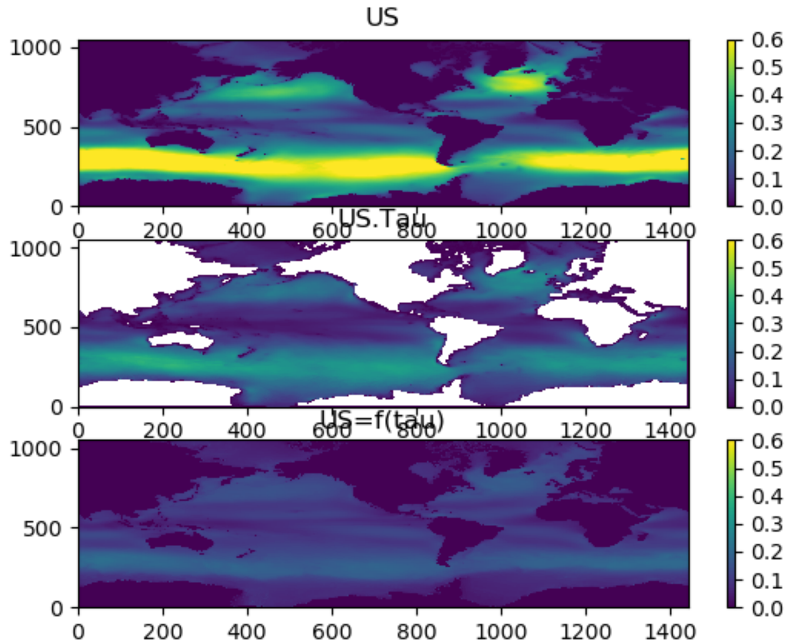

Figure 2. Annual average of surface Stokes drift module $\|\mathbf{u}^s(\eta)\|$ (top), of the portion of the Stokes drift aligned with the wind, as given in (16) (middle), and of the surface Stokes drift as parameterized by $0.377\sqrt{\|\boldsymbol{\tau}^{\mathrm{oce}}\|/\rho_0}$ in the uncoupled case (bottom)

3 Modeling system and coupling strategy

Our coupled model is based on the NEMO oceanic model, the WW3 wave model, and the OASIS library for ~~data exchanges and synchronizations~~ the data exchange and synchronization between both components.

3.1 Numerical models and coupling infrastructure

The ocean model : NEMO

NEMO is a state-of-the-art primitive-equation, split-explicit, free-surface oceanic model whose equations are formulated both in the vector invariant and flux forms (see (1) for the vector invariant form). The equations are discretized using a generalized vertical coordinate featuring, among others, the ~~z^*~~ $z^\star$-coordinate with partial step bathymetry and the σ-coordinate as well as a mixture of both (Madec, 2012). For efficiency and accuracy in the representation of external gravity waves propagation, model equations are split between a barotropic mode and a baroclinic mode to allow the possibility to adopt specific numerical treatments in each mode. The NEMO equations are spatially discretized on an Arakawa C-grid in the horizontal and a Lorenz grid in the vertical, and the time dimension is discretized using a Leapfrog scheme with a modified Robert-Asselin filter to damp the spurious numerical mode associated with Leapfrog (Leclair and Madec, 2009). For the current study the NEMO equations have been modified to include wave effects as described in (7) and (13). Moreover the modifications to the standard NEMO 1-equation TKE closure scheme are given in Sec. 2.3.

The wave model : WW3

The NEMO ocean model has been coupled to the WW3 wave model. In numerical models, waves are generally described using several phase and amplitude parameters. We provide here only the few sufficient details to understand the coupling of waves with the oceanic model, an exhaustive description of WW3 can be found in is given by The WAVEWATCH III® Development Group (2016). WW3 integrates the wave action equation (Komen et al., 1994), with the spectral density of wave action $N_\mathrm{w}(k_\mathrm{w},\theta_\mathrm{w})$, discretized in wavenumber k_w and wave propagation direction θ_w for the spectral space (subscripts w are used here to avoid confusion with previously introduced notations).

$$\partial_t N_\mathrm{w} + \partial_\phi \left(\dot{\phi} N_\mathrm{w}\right) + \partial_\lambda \left(\dot{\lambda} N_\mathrm{w}\right) + \partial_{k_\mathrm{w}} \left(\dot{k_\mathrm{w}} N_\mathrm{w}\right) + \partial_{\theta_\mathrm{w}} \left(\dot{\theta_\mathrm{w}} N_\mathrm{w}\right) = \frac{S}{\sigma}, \tag{17}$$

where λ is longitude, ϕ is latitude, and S is the net spectral source term that includes the sum of rate of change of the surface elevation variance due to interactions with the atmosphere via wind-wave generation and swell dissipation (S_atm), nonlinear wave-wave interactions interaction (S_nl), and interactions interaction with the upper ocean that is generally dominated by wave breaking (S_oc). Those parameterized source terms are important in waves-ocean coupling. Indeed, as shown earlier in (15) the S_oc term is used to compute the TKE flux transmitted to the ocean, and the S_in term enters in the computation of the wave-supported stress. They are here computed following Ardhuin et al. (2010b). In (17), the dot variables correspond to a propagation speed given by

$$\dot{\phi} = \left(c_g \cos\theta_\mathrm{w} + v|_{z=\eta}\right) R^{-1} \tag{18}$$

$$\dot{\lambda} = \left(c_g \sin\theta_\mathrm{w} + u|_{z=\eta}\right) (R\cos\phi)^{-1} \tag{19}$$

$$\dot{\theta_\mathrm{w}} = c_g \sin\theta_\mathrm{w} \tan\phi R^{-1} + \sin\theta_\mathrm{w} \frac{\partial\omega}{\partial\phi} \frac{\partial\omega_\mathrm{w}}{\partial\phi} - \frac{\cos\theta_\mathrm{w}}{\cos\phi} \frac{\partial\omega}{\partial\lambda} \frac{\partial\omega_\mathrm{w}}{\partial\lambda} (k_\mathrm{w} R)^{-1} \tag{20}$$

$$\dot{k_\mathrm{w}} = -\frac{\partial\sigma}{\partial H} \frac{\mathbf{k}}{k_\mathrm{w}} \cdot \boldsymbol{\nabla} D - \mathbf{k} \cdot \boldsymbol{\nabla} \mathbf{u}_h(z=\eta), \tag{21}$$

where R is earth radius, $\mathbf{u}_h(z=\eta) = (u|_{z=\eta}, v|_{z=\eta})$ are the surface currents provided by the ocean model, c_g is the group velocity, ω ω_w the absolute radian frequency, and H the mean water depth. Equation (17) is solved for each spectral component $(k_\mathrm{w},\theta_\mathrm{w})$ which are coupled by the advection and source terms. Equations (18)-(21) show how the oceanic currents affect the advection of the wave action density, there are also indirect effects via the source term (Ardhuin et al., 2009).

The coupler : OASIS3-MCT

The practical coupling between NEMO and WW3 has been implemented using the OASIS3-MCT (Valcke, 2012; Craig et al., 2017) software primarily developed for use in multi-component climate models. This software provides the tools to couple various models at low implementation and performance overhead. In particular, thanks to MCT (Jacob et al., 2005), it includes the parallelization of the coupling communications and runtime grid interpolations. For efficiency, interpolations are formulated in the form of a matrix-vector multiplication where the matrix containing the mapping weights is computed offline ~~one~~ once for all. In practice, after compiling OASIS3-MCT, the resulting library is linked to the component models so that they have access to the specific interpolation and data exchange subroutines. Now that we have described the different components involved in our coupled system, we go into the details of the nature of the data exchanged between both models.

3.2 Oceanic surface momentum flux computation

Surface waves affect the momentum exchange between the ocean and the atmosphere in two different ways. First the modification of surface rugosity acts on the incoming atmospheric momentum flux $\boldsymbol{\tau}^{\mathrm{atm}}$. Second, ~~even if most~~ a part of the momentum flux ~~going into the waves is quickly transferred to the water column through wave breaking (we call this portion $\boldsymbol{\tau}^{\mathrm{oce}}$), a part of it is~~ from the atmosphere is consumed by the wave field and contributes to the growing waves (the so-called wave-supported stress) and conversely the waves release momentum to the ocean when they break and dissipate. This implies that the wind-stress transferred to the oceanic model (we call it $\boldsymbol{\tau}^{\mathrm{oce}}$) is different from the atmospheric wind-stress $\boldsymbol{\tau}^{\mathrm{atm}}$. These two coupling processes are taken into account in our coupled framework.

The 10 meters wind $\mathbf{u}_{10}^{\mathrm{atm}}$ is sent to the wave model ~~and used to~~ which internally computes the dimensionless Charnock parameter α_{ch} characterizing the sea surface roughness (Charnock, 1955; Janssen, 2009). Those informations are used by the wave model to compute compute its own atmospheric wind-stress $\boldsymbol{\tau}_{\mathrm{ww3}}^{\mathrm{atm}}$ assuming neutral stratification, i.e. ~~$\boldsymbol{\tau}_{\mathrm{ww3}}^{\mathrm{atm}} = \rho_a C_{\mathrm{DN}} \|\mathbf{u}_{10}^{\mathrm{atm}}\| \mathbf{u}_{10}^{\mathrm{atm}}$~~ $\boldsymbol{\tau}_{\mathrm{ww3}}^{\mathrm{atm}} = \rho_a C_{\mathrm{DN}}(\alpha_{\mathrm{ch}}) \|\mathbf{u}_{10}^{\mathrm{atm}}\| \mathbf{u}_{10}^{\mathrm{atm}}$ with C_{DN} a neutral drag coefficient which is function of the Charnock parameter. Then the wave model computes the momentum flux transferred to the ocean $\boldsymbol{\tau}_{\mathrm{ww3}}^{\mathrm{oce}}$ ~~as well as the dimensionless Charnock parameter α_{ch} which characterizes the sea surface roughness (Charnock, 1955; Janssen, 2009)~~. Using the latest available values of α_{ch}, $\boldsymbol{\tau}_{\mathrm{ww3}}^{\mathrm{atm}}$, $\boldsymbol{\tau}_{\mathrm{ww3}}^{\mathrm{oce}}$, and $\mathbf{u}_{10}^{\mathrm{atm}}$, the oceanic model computes an atmospheric wind-stress $\boldsymbol{\tau}^{\mathrm{atm}}$ using its own bulk formulation and the local value of the momentum flux going into the water column is

$$\boldsymbol{\tau}^{\mathrm{oce}} = \boldsymbol{\tau}^{\mathrm{atm}} - (\boldsymbol{\tau}_{\mathrm{ww3}}^{\mathrm{atm}} - \boldsymbol{\tau}_{\mathrm{ww3}}^{\mathrm{oce}}) \tag{22}$$

where the $\boldsymbol{\tau}_{\mathrm{ww3}}$ quantities are interpolated from the wave grid to the oceanic grid. In NEMO, the wind-stress is computed using the IFS[3] bulk formulation such as implemented in the AeroBulk[4] package (Brodeau et al., 2016). In particular the roughness length which enters in the definition of the drag coefficient is function of the Charnock parameter α_{ch}

$$z_0 = \alpha_{\mathrm{ch}} \frac{u_\star^2}{g} + \alpha_m \frac{\nu}{u_\star}$$

where $\alpha_m = 0.11$, $u_\star$ is the friction velocity, and ν the air kinematic viscosity whose contribution is significant only asymptotically at very low wind speed. Note that in the uncoupled case the default value of the Charnock parameter is $\alpha_{\mathrm{ch}}^0 = 0.018$. In our implementation, the momentum fluxes are computed using the absolute wind $\mathbf{u}_{10}^{\mathrm{atm}}$ at $10\mathrm{m}$ rather than the relative wind

[3] Integrated Forecasting System: https://www.ecmwf.int/en/forecasts/documentation-and-support/changes-ecmwf-model/ifs-documentation

[4] http://aerobulk.sourceforge.net/

$\mathbf{u}_{10}^{\mathrm{atm}} - \mathbf{u}_h(z=\eta)$. Indeed, several recent studies have emphasized that the use of relative winds is relevant only when a full coupling with an atmospheric model is available since in a forced mode it leads to an unrealistically large loss of oceanic eddy kinetic energy (e.g. Renault et al., 2016). This is not a limitation of our approach since a simple modification of a namelist parameter allows to run with relative winds but this case is not investigated in the present study.

~~Note that in~~ In our coupling strategy two different values of the atmospheric wind-stress and of the wave to ocean wind stress are computed with two different bulk formulations. This strategy is not fully satisfactory since it breaks the momentum conservation. However, it was necessary in practice since the WW3 results were very sensitive to the bulk formulation and at the same time it was not conceivable to use the WW3 bulk formulation to force the ocean model because the latter ignores the ~~effects~~ effect of stratification in the atmospheric surface layer. Previous implementations in NEMO ~~(e.g. Breivik et al., 2015; Alari et al., 2016; Staneva et al., 2017; Law Chune and Aouf, 2018)~~ (e.g. Breivik et al., 2015; Alari et al., 2016; assumed that the wave field only acts on the norm of $\boldsymbol{\tau}^{\mathrm{atm}}$ and not on its orientation. Instead of (22), the atmospheric wind stress was corrected as follow:

$$\boldsymbol{\tau}^{\mathrm{oce}} = \boldsymbol{\tau}^{\mathrm{atm}} \left(\frac{\boldsymbol{\tau}_{\mathrm{ww3}}^{\mathrm{oce}}}{\boldsymbol{\tau}_{\mathrm{ww3}}^{\mathrm{atm}}} \right)$$

However, this approach potentially leads to artificially large values of $\boldsymbol{\tau}^{\mathrm{oce}}$ when $\boldsymbol{\tau}_{\mathrm{ww3}}^{\mathrm{atm}}$ is small and it does not take into account the slight change in $\boldsymbol{\tau}^{\mathrm{oce}}$ direction induced by the waves.

3.3 Additional details about the practical implementation

In Table 1 the different variables exchanged between the oceanic and wave models are given. All variables are 2D variables meaning that no 3D arrays are exchanged through the coupler. All 2D interpolation are made through a distance weighted bilinear ~~interpolations~~interpolation. The time discretization steps Δt_{ww3} for WW3 and Δt_{nemo} for NEMO are generally different with $\Delta t_{\mathrm{ww3}} > \Delta t_{\mathrm{nemo}}$ and chosen such that $\Delta t_{\mathrm{ww3}} = n_t \Delta t_{\mathrm{nemo}}$ ($n_t \in \mathbb{N}, n_t \geq 1$). In this case, coupling fields from NEMO to WW3 are averaged in time between two exchanges, while fields from WW3 to NEMO are sent every Δt_{ww3} steps and therefore updated every n_t time steps in NEMO. If $\Delta t_{\mathrm{ww3}} > \Delta t_{\mathrm{nemo}}$, the coupler time-step is set to Δt_{ww3}. ~~Note that our~~ Our current implementation does not include an explicit coupling between waves and sea-ice while it is known that waves lead to ice break-up, pancake ice formation and associated enhancement of both freezing and melting and, in return, this wave dissipation in ice-covered water (e.g. Stopa et al., 2018) leads to ice drift. Such explicit coupling is currently under development within the NEMO framework (Boutin et al., 2019).

Variable	description		units	
$\mathbf{u}_h(z=\eta)$	Oceanic surface currents	O→W	$\mathrm{m\,s^{-1}}$	
$\mathbf{u}_{10}^{\mathrm{atm}}$	$10\ \mathrm{m}$-winds from external dataset	O→W	$\mathrm{m\,s^{-1}}$	-
$\mathbf{u}_h^s(z=\eta)$	Sea-surface Stokes drift	W→O	$\mathrm{m\,s^{-1}}$	
$\Vert\mathbf{T}^s\Vert$	norm of the Stokes drift volume transport	W→O	$\mathrm{m^2\,s^{-1}}$	
Φ_{oc}	TKE surface flux multiplied by ρ_0	W→O	$\mathrm{W\ m^{-2}}$	
α_{ch}	Charnock parameter	W→O	-	
$\boldsymbol{\tau}_{\mathrm{w}}^{\mathrm{ww3}}$	Wave-supported stress	W→O	$\mathrm{N.m^{-2}}$	
$\widetilde{p}^J$	wave-induced pressure	W→O	$\mathrm{m^2\,s^{-2}}$	
H_s	Significant wave height	W→O	m	

Table 1. Variables exchanged between NEMO (O) and WW3 (W) via the OASIS3-MCT coupler. The $10\ \mathrm{m}$ wind $\mathbf{u}_{10}^{\mathrm{atm}}$ is interpolated online by WW3 and does not go through the OASIS3-MCT coupler.

4 Global $1/4^o$ coupled wave-ocean simulations

4.1 Experimental setup and experiments

4.1.1 The global coupled ORCA25 configuration

The wave hindcasts presented here are all based on the WW3 model in its version 6.02 configured with a single grid at 0.5^o resolution in longitude and latitude. A spectral grid with 24 directions and 31 frequencies exponentially spaced over the interval $[f_{\min}, f_{\max}]$ with $f_{\min} = 0.037$ Hz and $f_{\max} = 0.7$ Hz. A one-step monotonic third-order coupled space-time advection scheme (a.k.a. Ultimate Quickest scheme) is used with a specific procedure to alleviate the so-called garden sprinkler effect (Tolman et al., 2002). As suggested in Phillips (1984), the dissipation induced by wave breaking is proportional to the local saturation spectrum (see also Ardhuin et al., 2010a; Rascle and Ardhuin, 2013). The wind input growth rate at high ~~frequencies~~ frequency is based on the formulation of Janssen (1991) with an additional "sheltering" term to reduce the effective winds for the shorter waves (Chen and Belcher, 2000; Banner and Morison, 2010). For the computation of nonlinear wave-wave interactions, the discrete interaction approximation of Hasselmann et al. (1985) is used. This last approximation is known to be inaccurate but it is thought that the associated error are usually compensated by a proper adjustment of the dissipation source term (Banner and Young, 1994; Ardhuin et al., 2007). As mentioned earlier in Sec. 3.2, the model was run with 10 meter winds, without any air-sea stability correction. No wave measurements were assimilated in the model but the stand-alone wave model was developed based on spectral buoy and SAR data (Ardhuin et al., 2010b), and calibrated against altimeter data by adjusting the wind-wave coupling parameter (Rascle and Ardhuin, 2013). The WW3 time-step for the global configurations is $\Delta t_{\mathrm{ww3}} = 3600\ \mathrm{s}$.

For the oceanic component, we use a global ORCA025 configuration at a $1/4^o$ horizontal resolution (Barnier et al., 2006). The vertical grid is designed with 75 vertical z-levels with vertical spacing increasing with depth. Grid thickness is about $1\ \mathrm{m}$

near the surface and increases with depth to reach 200 m at the bottom. Partial steps are used to represent the bathymetry. The LIM3 sea-ice model is used for the sea-ice dynamics and thermodynamics (Rousset et al., 2015). The vertical mixing coefficients are obtained from the 1-equation TKE scheme described in Sec. 2.3 and the convective processes are mimicked using an enhanced vertical diffusion parameterization which increases vertical diffusivity to 10 $m^2\,s^{-1}$ where static instability occurs. Water density is computed from temperature and salinity through the use of a polynomial formulation of the UNESCO (1983) non-linear equation of state (Roquet et al., 2015).~~The numerical options are the one commonly chosen by the Drakkar group~~[5]~~. The~~ The vector-invariant form momentum advection is using Arakawa and Lamb (1981) for the vorticity and a specific formulation to control the Hollingsworth instability (Ducousso et al., 2017). Momentum lateral viscosity is biharmonic and acts along geopotential surfaces. It is set to a value of 1.5×10^{11} $m^4.s^{-1}$ at the equator and vary proportionally to Δx^3 away from the equator. Advection of tracers is performed with a flux-corrected-transport (FCT) scheme (Lévy et al., 2001), and lateral diffusion of tracers is harmonic and acts along iso-neutral surface. It is set to a value of 300 $m^2\,s^{-1}$ at the equator which varies proportionally to Δx. The bottom friction is non-linear and the lateral boundary condition is free-slip. In this setup, the baroclinic time step is set to $\Delta t_{\mathrm{nemo}} = 900$s, and a barotropic time step 30 times smaller. All experiments were initialised from GLORYS2V4 reanalyses (www.mercator-ocean.fr). Compared to the standard uncoupled ORCA025 configuration, the additional computational cost associated to WW3 and to the exchanges through the coupler is about 20%.

4.1.2 Atmospheric forcings

The atmospheric fields used to force both ocean and wave models are based on the ECMWF (European Centre for Medium-Range Weather Forecasts) ERA-Interim reanalysis (Dee et al., 2011). Corrections have been applied to ~~better reproduce the diurnal cycle of forcing fields and to~~ guarantee that the ERA-Interim mean state for rainfalls, shortwave and longwave radiative fluxes are consistent with satellite observations from Remote Sensing Systems (RSS) Passive Microwave Water Cycle (PMWC) product (Hilburn, 2009) and GEWEX SRB 3.1 data[5]. Momentum and heat turbulent surface fluxes are computed using the IFS bulk formulation from AeroBulk package (Brodeau et al., 2016) using air temperature and humidity at 2 meters, mean sea level pressure and 10 meter winds.

4.1.3 Sensitivity experiments and objectives

Sensitivity experiments have been conducted to check the proper implementation of various components of the present coupled modelling system. For the sake of clarity, our developments are split in four components: *(i)* the modification of the wind-stress by waves through the Charnock parameter and the inclusion of wave-supported stress, *(ii)* the modifications of the NEMO governing equations through the Stokes-Coriolis, Vortex force and wave-induced surface pressure terms, *(iii)* the addition of a Langmuir turbulence parameterization, and *(iv)* the modifications to the TKE scheme. As summarized in Tab. 2, sensitivity experiments are designed in such a way to incrementally increase the level of complexity and test the effect of each component.

[5]

[5] http://gewex-srb.larc.nasa.gov/common/php/SRB_data_products.php

Case	O-W coupling	Wave-supported stress + Charnock parameter	$\mathcal{W}_{\mathrm{St-Cor}}$, $\mathcal{W}_{\mathrm{VF}}$, $\mathcal{W}_{\mathrm{Prs}}$	Langmuir cells parameterization(rn_lc)	Modified TKE scheme
No_CPL	no	no	no	no	no
WS_CPL	2-way	yes	no	no	no
ST_CPL	2-way	yes	yes	no	no
TKE_CPL	2-way	yes	yes	no	yes
All_CPL1	2-way	yes	yes	yes (0.15)	yes
All_CPL2	2-way	yes	yes	yes (0.30)	yes

Table 2. Various model configurations analyzed in Sec. 4.2.

The No_CPL experiment corresponds to the classical NEMO setup where wave effect is parameterized through a wind-stress dependent TKE surface boundary condition as suggested by Craig and Banner (1994). In this approach, a Dirichlet surface boundary condition is used and expressed as follow: $e(z=\eta) = \frac{1}{2}(15.8\alpha_{CB})^{2/3}\frac{\|\boldsymbol{\tau}^{\mathrm{atm}}\|}{\rho_0}$ with $\alpha_{CB} = 100$. Based on the results of Mellor and Blumberg (2004) we expect that in the uncoupled case the nature of the boundary condition (i.e. Dirichlet vs Neumann) does not significantly impact numerical solutions[6]. The WS_CPL ~~expriment~~ experiment is identical as No_CPL except that the wave coupling is introduced within the wind-stress computation, as described in Sec. 3.2. ST_CPL experiment is as WS_CPL except that all terms relative to the Stokes drift described in Sec. 2.1 are added in NEMO. TKE_CPL corresponds to ST_CPL but with the modified TKE scheme described in 2.3.1. All_CPL(1&2) experiments are like ~~ST_CPL~~ TKE_CPL but with a fully modified TKE scheme including the Langmuir cells parameterization described in 2.3.2. All those simulations have been performed for 2 years (2013-2014) where 2013 is let as spinup and only 2014 is analysed. ~~It~~ We considered 2 years were enough to illustrate the fact that our developments were actually producing the expected results. Integrating longer in time could also lead to drifts in the stratification independently from the wave effects and could thus distort our interpretation. In any case, it must be clear that the objective here is not to go through a thorough physical analysis of coupled solutions but to check and validate our numerical developments.

4.2 Numerical results

4.2.1 Waves impact on oceanic Wind stress

The wave distribution being inhomogeneous on the globe, it is expected that with the wave-modified wind stress ~~parametrization~~ parameterization the stress should follow more closely the wave patterns. In Fig. 3, the seasonal ~~averages~~ average of the significant wave height and of the ~~differences~~ difference between the Charnock coefficient computed by the wave model and the default constant value used in the uncoupled case ($\alpha^0_{\mathrm{ch}} = 0.018$) are shown. As expected, the Charnock parameter tends to

[6] In Mellor and Blumberg (2004) the authors consider a Dirichlet boundary condition such that $e(z=\eta) = \frac{1}{2}(15.8\alpha_{CB})^{2/3}u_\star^2$ and an equivalent Neumann condition $K_e\partial_z e|_{z=\eta} = 2\alpha_{CB}u_\star^3$. The authors claim that numerical solutions using a Dirichlet condition instead of a Neumann condition are qualitatively similar.

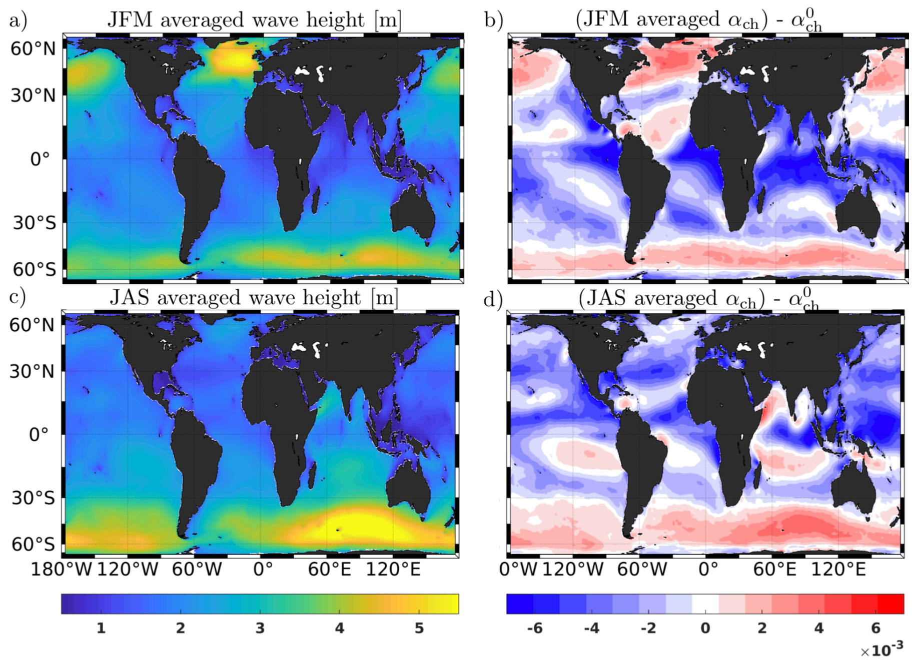

Figure 3. (a&c):Seasonal averaged averages of Significant wave height (in meters) for January February March (JFM, panel a) and July August September (JAS, panel c). (b&d):Seasonal Averaged differences average of the difference between the Charnock parameter as computed by the wave model and the default value $\alpha^0_{ch} = 0.018$ for JFM (panel b) and JAS (panel d).

be stronger in the area where the waves are the higher. Generally an increase of the Charnock parameter is observed in the northern and southern basin while there is a net decrease of α_{ch} near the equator. There is also a strong seasonality in the north northern hemisphere with a reduction in summer and a strong increase in winter. The differences between α_{ch} and α^0_{ch} are very latitudinal with very few longitudinal variations.

To isolate the effect of the Charnock parameter we compare the results obtained in the No_CPL and WS_CPL experiments. Those two experiments show relatively similar sea surface temperature patterns meaning that the modifications modification of the wind-stress $\|\boldsymbol{\tau}^{\rm oce}\|$ between those two cases are is primarily due to the use of different Charnock parameters and the inclusion of the wave-supported stress. Fig. 4 (panel a) illustrates that the Charnock parameter mostly affects the drag coefficient C_D, hence the surface wind-stress, for large winds. The ocean-wave coupling does not lead to appreciable differences in the drag coefficient C_D for wind speeds lower than $8\ \mathrm{m\,s^{-1}}$. On the contrary, since large values of the Charnock parameter are observed for large wind speeds, the coupling significantly increases the drag (as well as its variance) at high winds. Fig. 4 (panel b) shows how the wind-stress is modified by this increase of the drag coefficient jointly with the wave-supported stress which tends to decrease the wind-stress magnitude (Fig. 5). At low wind speed the wind-stress magnitude is not affected by the coupling with waves while for strong winds the increase of wind-stress associated with the increased drag coefficient is always larger than the decrease associated to the wave-supported stress. This latter effect reduces the wind stress by no more

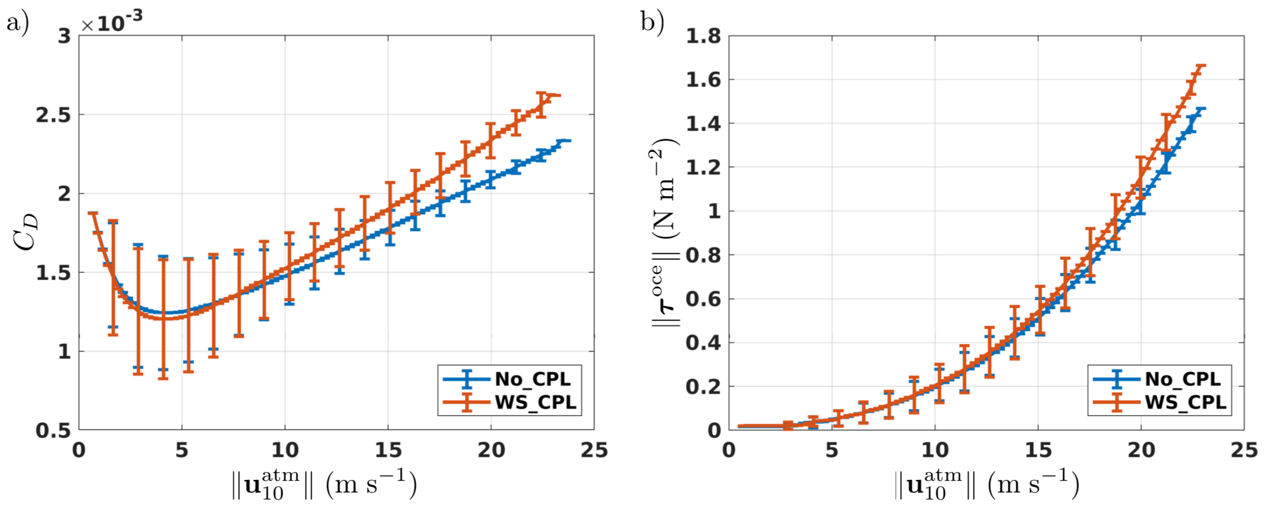

Figure 4. (a) Drag coefficient (C_D) as a function of the 10 meters wind speed $\|\mathbf{u}_{10}^{\mathrm{atm}}\|$ and (b) Wind Stress norm $\|\boldsymbol{\tau}^{\mathrm{oce}}\|$ as a function of $\|\mathbf{u}_{10}^{\mathrm{atm}}\|$ (Black curves represent the mean value while the vertical bars represent the standard deviation.)

than 2%, for the characteristic scales of our study, this correction is thus almost negligible. The wind-stress changes due to the coupling with waves seen in our simulations are very localized in time and space and it is thus difficult to conclude on their overall effect on the upper ocean dynamics such as the Ekman pumping and the surface currents.

4.2.2 Waves impact on surface TKE injection

As described in section 2.3, in the ocean-waves coupled case, the surface boundary condition for the TKE equation is a Neumann condition whose value is directly given by the wave model, unlike the uncoupled case where a Dirichlet condition is imposed. We aim here at assessing the impact on the order of magnitude of the near-surface TKE. Since the Neumann boundary condition is applied at the center of the top-most grid box (i.e. approximately at $50\,\mathrm{cm}$ depth), we compare in Fig. 6 the TKE value at 1 meter depth between the coupled (All_Cpl2) and the uncoupled (No_CPL) case. Positive values means that near-surface TKE is larger in the coupled simulation. It shows an almost homogeneous increase of the TKE (up to more than 100%) in the extra-tropical areas. While low seasonal variability in the extra-tropical areas is visible in Fig. 6, a spatial averaging by hemisphere (Fig. 7) highlights seasonal variability with a strong increase in both near-surface TKE value and TKE difference between both experiments during winter. In Fig. 6, 7 (and also in the reminder of the paper), the spatial averaging is made between $25\,\mathrm{S}$ and $60\,\mathrm{S}$ in the southern hemisphere and between $25\,\mathrm{N}$ and $60\,\mathrm{N}$ in the northern hemisphere to avoid any conflicts with sea-ice and to remove the equatorial region from the comparison. The increase of the surface TKE injection associated with waves is expected to contribute to an overall increase of mixed layer depth provided that the mixing length diagnosed by the turbulent closure scheme allows to effectively propagate this additional TKE deeper in the mixed layer.

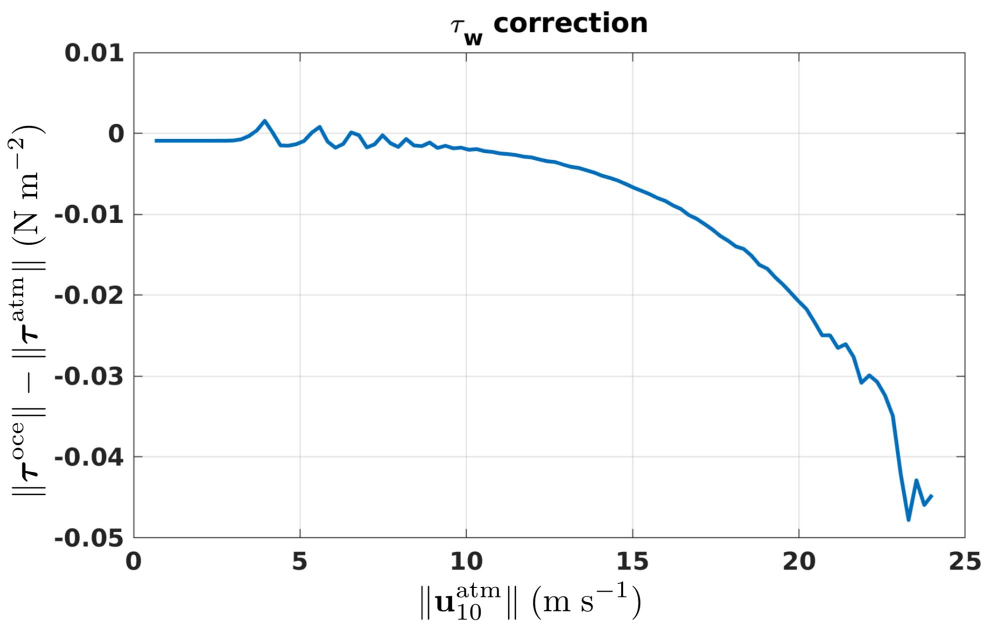

Figure 5. Wind-stress difference $\|\boldsymbol{\tau}^{\mathrm{oce}}\| - \|\boldsymbol{\tau}^{\mathrm{atm}}\|$ (N m^{-2}) due to the correction made for growing waves for the WS_CPL experiment, as a function of the 10 meters wind speed.

4.2.3 Waves impact on Mixed layer depth

In this section, we evaluate the wave effect on vertical mixing using the mixed layer depth (MLD) as a relevant metric. Fig. 8 represents the seasonally averaged difference in MLD between the coupled (All_CPL2) and the uncoupled (No_CPL) case relative to the No_CPL case (i.e. $(h_{\mathrm{mld}}^{\mathrm{nocpl}} - h_{\mathrm{mld}}^{\mathrm{cpl}})/h_{\mathrm{mld}}^{\mathrm{nocpl}}$ with h_{mld} considered negative downward). It shows a significant deepening of the mixed layer at high latitudes in the coupled case with only very few localized mixed layer shallowing up to 60% mainly in the southern hemisphere. To assess whether the overall deepening of the mixed layer is realistic, we make a comparison with available observations. Available observations for 2014 were extracted following an updated data set from de Boyer Montégut et al. (2004). The MLD depth as been computed as being the depth where the density is 3% smaller that the density at 10m as in de Boyer Montégut et al. (2004). Fig. 9 represents the spatially averaged MLD where the blue line is the spatially averaged MLD obtained from ARGO floats (available during the same period) in both hemispheres. In the northern hemisphere (Fig. 9, a), there is only a slight improvement compared to data during winter and late summer when implementing the coupling with waves. In the southern hemisphere (Fig. 9, b) the situation is rather different. From January to July, the deepening of MLD induced by the wave coupling significantly reduces the bias between the model and ARGO data. From July to December, results in the coupled case show an overestimation of MLDs which were already too deep in the uncoupled case, therefore increasing the bias between data and model. Since mesoscale activity make direct comparisons to data unreliable for such a short period of time, we compare the normalized distribution of MLD between the different simulations and available

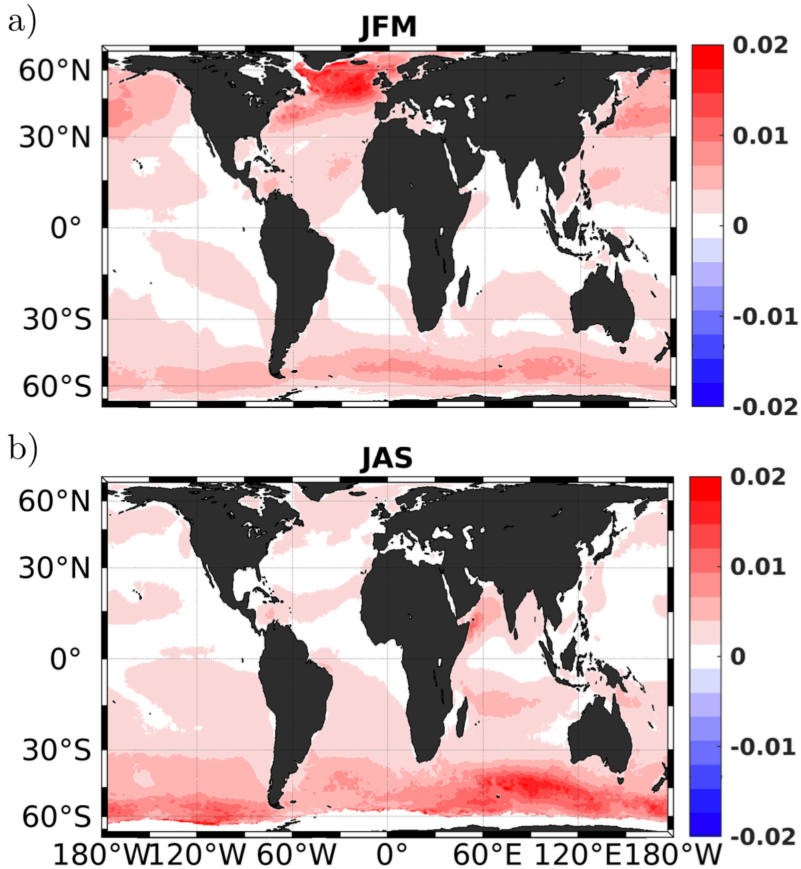

Figure 6. Seasonal ~~differences~~ difference of 1 meter depth turbulent kinetic energy ($\mathrm{m}^2\,\mathrm{s}^{-2}$) between the coupled case (All_Cpl2) and the uncoupled case (No_CPL). (a) for January, February, March (JFM) and (b) for July, August, September (JAS).

ARGO data. Results are presented in Fig. 10 for year 2014 (panel (a)) and during summer only (panel (b)). In both cases the ~~improvements~~ improvement in the northern hemisphere ~~are~~ is very modest. As far as the southern hemisphere is concerned the coupling with waves leads to a significant improvement compared to MLD derived from ARGO floats despite the fact that there are still too many low MLD values in the range $50-100$ m. In comparison with the uncoupled case there is a more realistic spreading toward deeper mixed layer depths. More particularly in summer (Fig. 10, b), the probability density function (PDF) in the coupled case matches almost perfectly the ~~ones~~ one computed from ARGO data. Despite the fact that we did not activate the *ad-hoc* extra mixing induced by near-inertial waves (Rodgers et al., 2014) our implementation of the wave-ocean interaction leads to a significant deepening of the MLD in a realistic way. To better understand which components of the wave-ocean coupling are responsible for this improvement, the summer PDF in the South hemisphere has been computed for each of the experiments described in Tab. 2. Results are shown in Fig. 11. First of all, it can be seen that all the wave-ocean retroactions described in previous sections lead to an improvement in terms of mixed layer depth distribution compared to the uncoupled

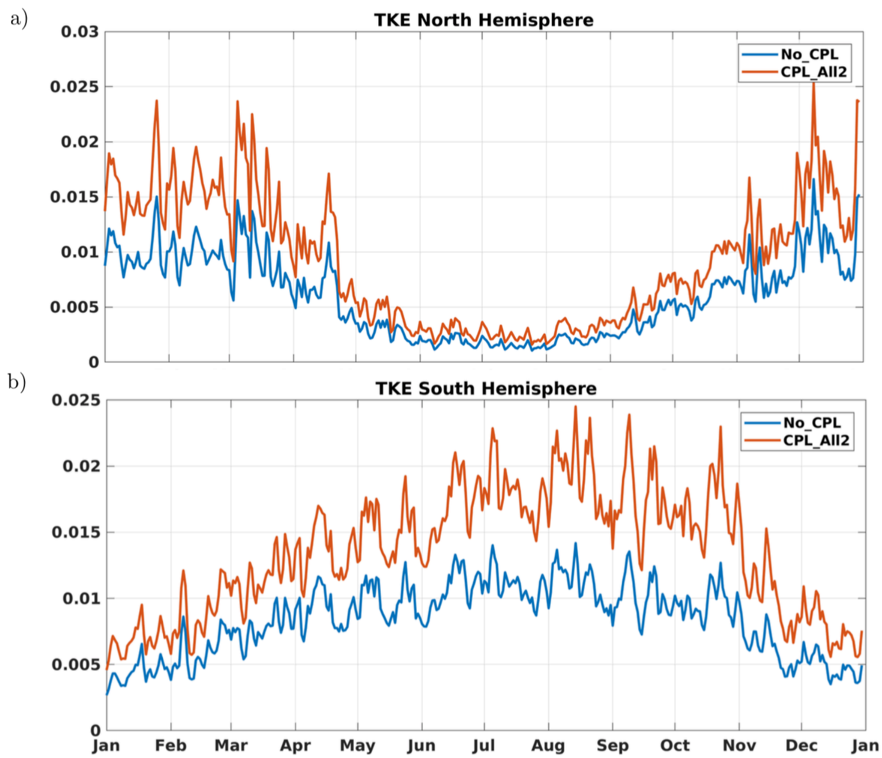

Figure 7. Spatially averaged turbulent kinetic energy ($m^2\ s^{-2}$) at one meter depth over (a) the Southern Hemisphere and (b) the Northern Hemisphere.

case. Indeed, the modification of the wind stress by the wave field introduced in WS_CPL, increases both surface currents and near surface TKE values resulting in a slight deepening of the MLD. Adding the Stokes drift related terms in the primitive equations contributes only modestly to the deepening of the MLD while most of the improvement results from the modified TKE scheme ~~and more specifically from~~ with some slight improvement when the Langmuir parameterization is activated. It is somewhat reassuring to see that the better agreement with ARGO data is obtained when all components of the coupling are activated.

4.2.4 Waves impact on sea-surface temperature

Since the near-surface mixing is strengthened by the coupling we can expect an impact on sea-surface temperature (SST). Fig. 12 represents the time series of SST for each hemisphere. The Northern hemisphere is characterized by a warm bias during summer with a very slight improvement when coupling with waves. In the Southern hemisphere (Fig. 12, b) the summer warm bias is reduced by half in the coupled simulation and a slight warming occurs during the winter. While the summer surface cooling might be linked to the mixed-layer deepening, the winter warming might be rather linked to advection as observed by Alari et al. (2016) for the Baltic sea. It could also result from an increased heat content during ~~winter~~ summer leading to higher

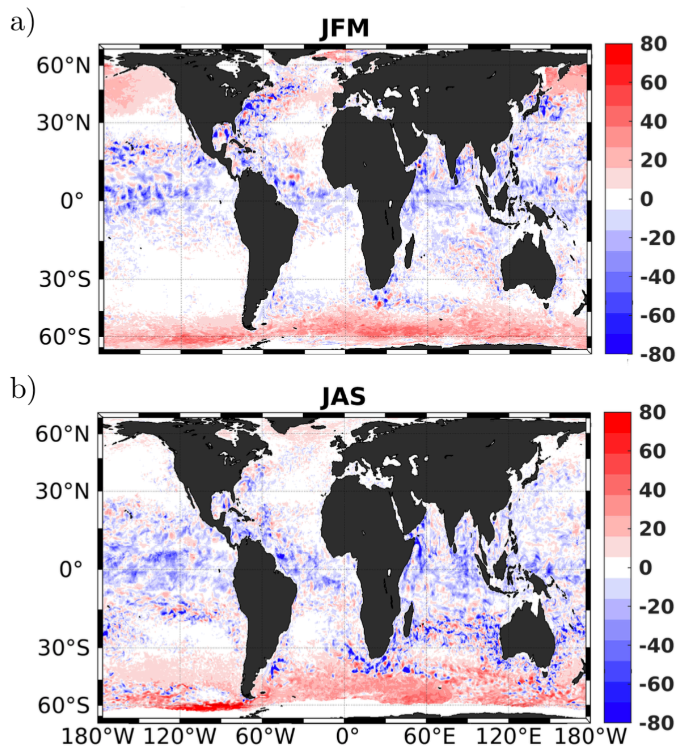

Figure 8. (a) & (b): Seasonaly averaged MLD differences (All_CPL2-No_CPL) relative to the uncoupled simulation No_CPL. Red color correspond to deeper MLD for All_CPL2.

SST during ~~summer~~winter. To better characterize the wave impact on the SST, we show in Fig. 13 (panel a) the difference in term of annual mean between the No_CPL experiment and OSTIA analysis exhibiting a cold bias in the No_CPL simulation in equatorial and tropical regions and a warm bias in the northern part of the Pacific ocean. The coupling with waves tends to diminish the cold bias (see Fig. 13, b) especially in the Pacific ocean and the warm bias in the north Pacific is significantly reduced. As already noticed by Law Chune and Aouf (2018) the warming in the equatorial and tropical regions mainly results from a lower wind stress caused by a value of the Charnock parameter lower than the value used in the uncoupled case (see Fig. 3,b,d). A consequence is a decrease of the drag coefficient leading to smaller turbulent exchange coefficients reducing the heat flux. As mentionned above, in extra-tropical regions, some warm bias tend to be partially reduced by the extra mixing induced by the waves at high latitude or/and by the increased turbulent transfer coefficient. The tendency of the wave coupling to improve the near-surface temperature distribution can also be verified on a time-latitude Hovmuller diagram like the ones shown in Fig. 14. For instance, it can be seen that the summer warm bias in the northern hemisphere (Fig. 14,a) coincides well with the cooling induced by the ~~waves coupling~~ coupling with waves (Fig. 14,b). Similarly we can also observe a warming in the tropical and equatorial regions (Fig. 14,b) corresponding to the cold bias seen in Fig. 14 (panel a). In the southern extra-tropical region, a summer cooling is observed. It is induced by the wave coupling whereas Fig. 14 (panel a) shows a slight

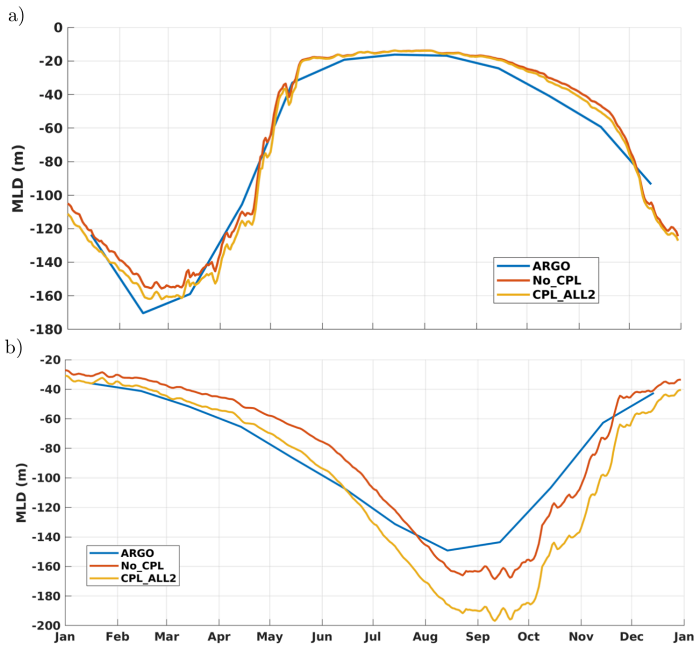

Figure 9. Spatially averaged MLD for (a) the north hemisphere and (b) the south hemisphere

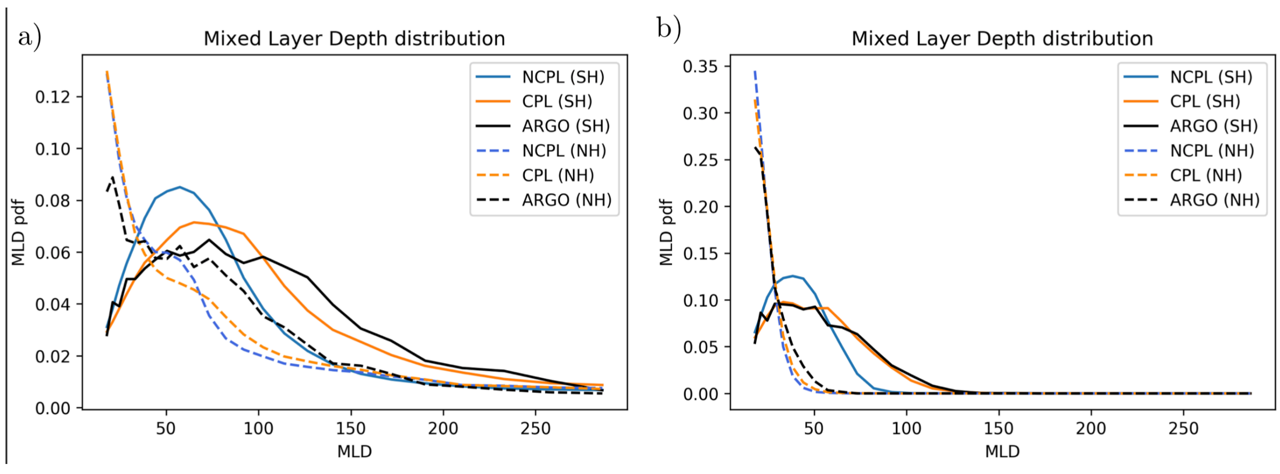

Figure 10. Mixed Layer Depth probability density function, for (a): the full 2014 year and (b): summer 2014.

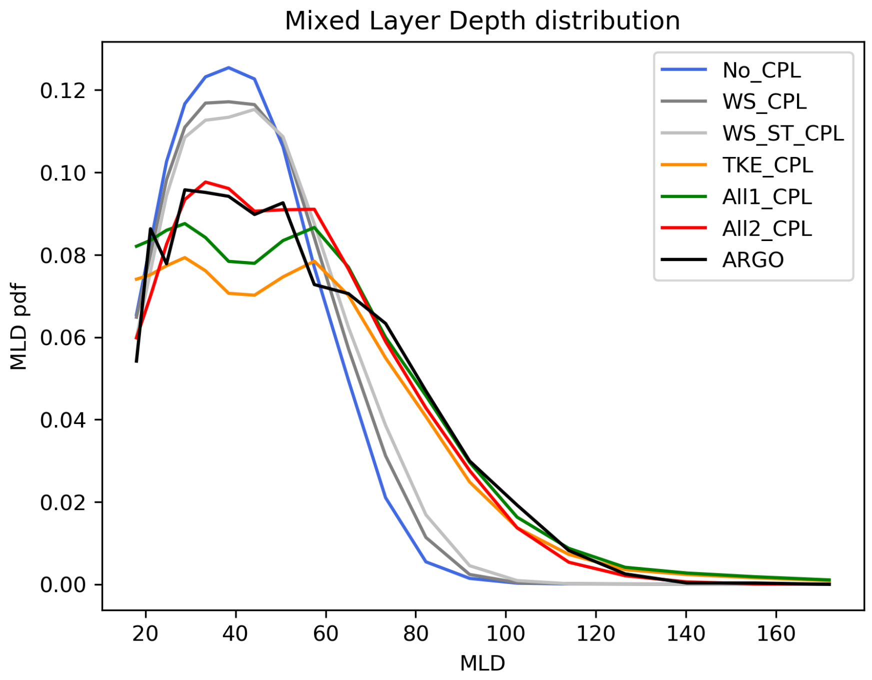

Figure 11. Mixed Layer Depth probability density function in the southern hemisphere during summer months. The details of each experiment can be found in Tab. 2.

warm bias. During winter we can observe north of 60 S a warming in Fig. 14 (panel b) which again partially corresponds to a cold bias in Fig. 14 (panel a).

4.2.5 Surface current and Kinetic Energy

The last aspect of our solutions we would like to evaluate is the impact of the surface waves on surface currents and kinetic energy (KE). To do so, we show in Fig. 15 time series of the spatially averaged surface kinetic energy for both hemispheres. Whatever the hemisphere there is a net decrease of surface KE (up to 20% in the south) when a coupling with the waves is included. This decrease of surface kinetic energy reflects a decrease of surface currents magnitude. Indeed, as detailed in Fig. 16 which represents the vertical profile of the horizontal components of the current in the oceanic surface boundary layer, the coupling with waves decreases both the surface currents magnitude and the shear. While currents from the WS_CPL are increased due to increased wind stress, the Stokes Coriolis force when included in momentum equations leads to a decrease of velocities in the whole boundary layer as previously shown by Rascle et al. (2008) (orange lines in Fig. 16). Inclusion of the vertical mixing due to waves and Langmuir circulation attenuates the currents in the surface layer, resulting in further reduced surface currents and stronger currents at the bottom of the boundary layer (purple lines in Fig. 16). This concludes our checking of the proper functioning of the coupling with waves as described in the present paper.

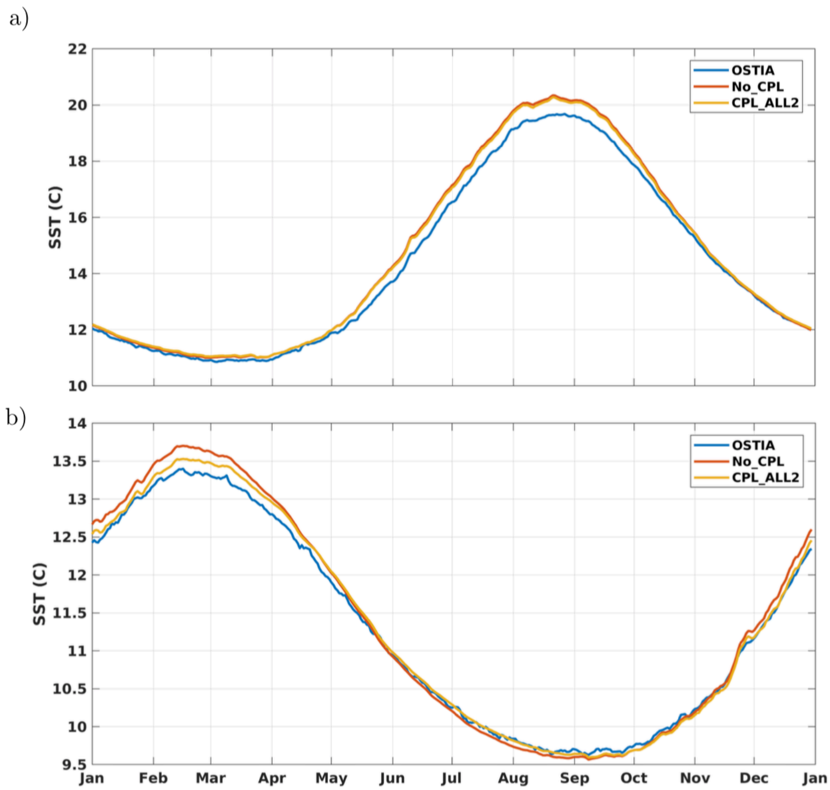

Figure 12. Time series of the spatially averaged Sea Surface Temperature (^{o}C); (a): North Hemisphere and (b): South Hemisphere

5 Conclusions

In this paper we have described the implementation of an online coupling between the oceanic model NEMO and the wave model WW3. The impact of such coupling on the model solutions has been assessed from the oceanic point of view for a global configuration. In particular, the following steps to set up the coupled model have been discussed in details (*i*) inclusion of all wave-induced terms in NEMO primitive equations, only neglecting the terms relevant for the surf zone which is outside the scope of the NEMO community, (*ii*) modification of the subgrid ~~scales~~ scale vertical physics (including the bulk formulation) to include wave effects and a parameterization of Langmuir turbulence, (*iii*) development of a coupling interface based on the OASIS3-MCT software for the exchange of data between both models, and (*iv*) tests of our developments on a realistic global configuration at $1/4°$ for the ocean coupled to a $1/2°$ resolution wave model. Compared to an ocean-only simulation, the coupling with a wave model (with a resolution twice coarser than the oceanic model) leads to an additional computational cost of about 20%.

Following McWilliams et al. (2004) and Ardhuin et al. (2008), in the weak vertical current shears limit, the wave-induced terms implemented in NEMO include the Stokes-Coriolis force, the vortex force, Stokes advection in tracer and continuity

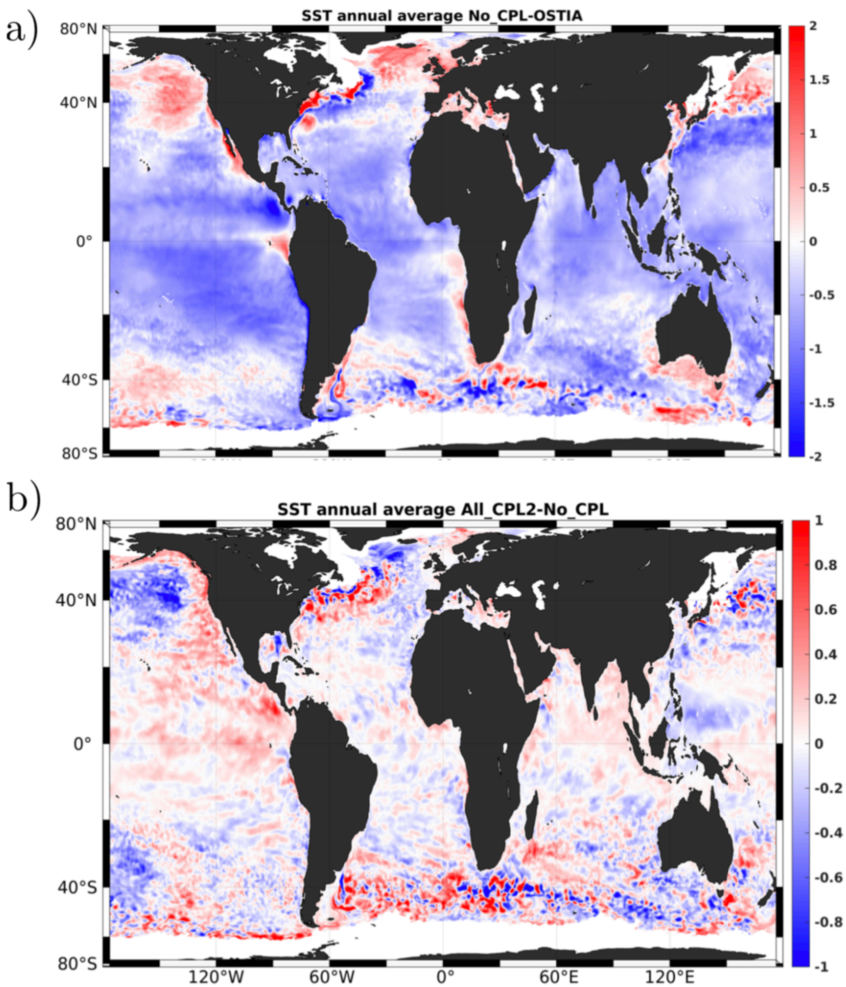

Figure 13. (a):Annual average of the differences between No_CPL and OSTIA sea surface temperatures (^{o}C) for year 2014 (positive when the model is warmer). (b):Annual average of the difference between All_CPL2 and No_CPL (positive when All_CPL2 is warmer)

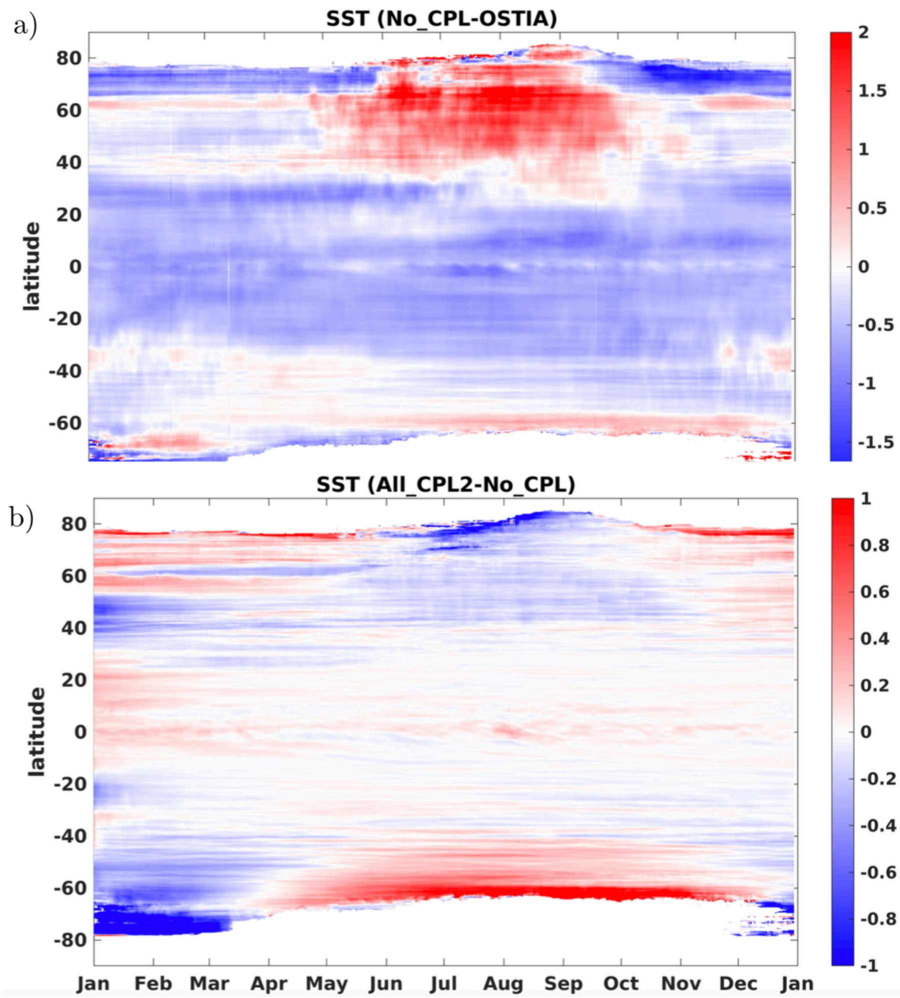

Figure 14. Hovmuller diagram of the longitudinally averaged sea surface temperature (°C) differences between (a): No_CPL and OSTIA and (b): between All_CPL2 and No_CPL.

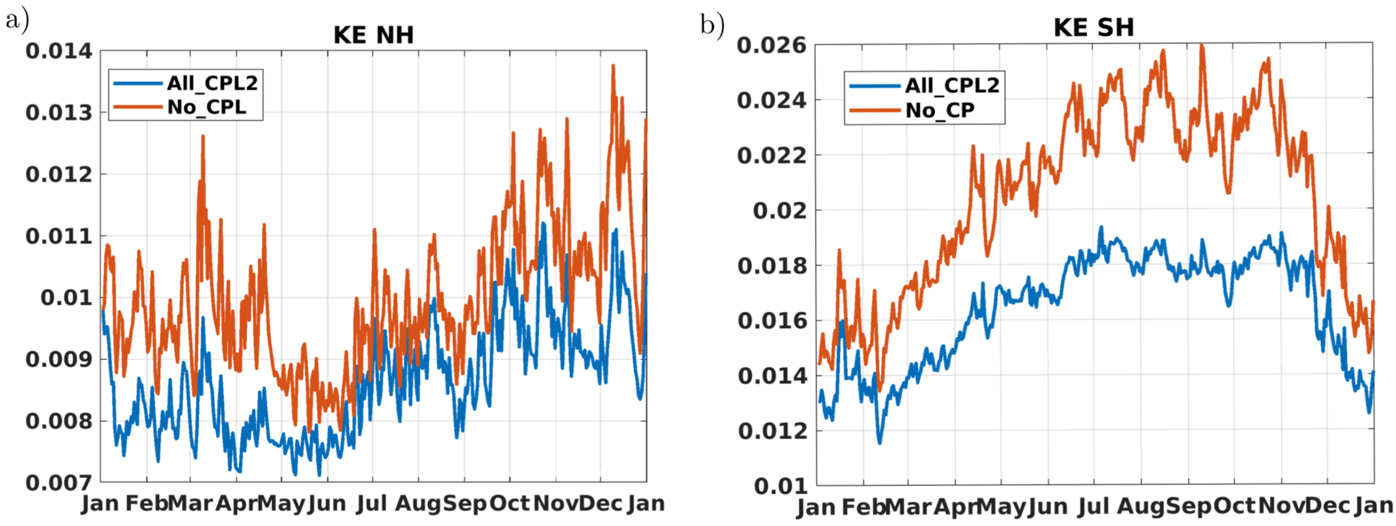

Figure 15. Time series of the spatially averaged surface kinetic energy ($\mathrm{m}^2\,\mathrm{s}^{-2}$) for (a): the Northern hemisphere and (b) the Southern hemisphere

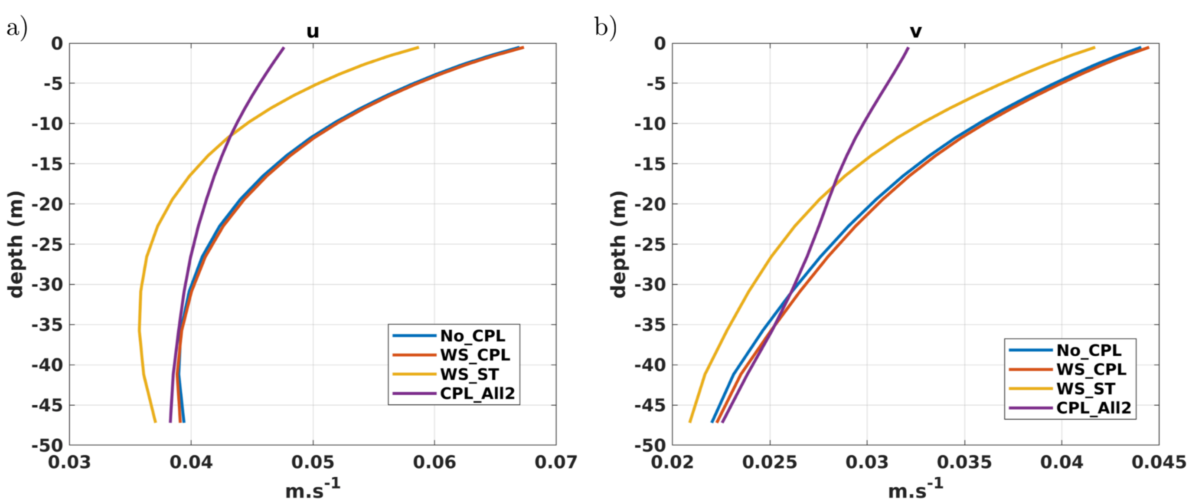

Figure 16. Zonally averaged zonal (a) and meridional (b) currents ($\mathrm{m\,s}^{-1}$) between 60 S and 25 S as a function of depth (m) for the simulations described in Tab. 2.

equations as well as a wave-induced surface pressure term. The prognostic equation for TKE also includes an additional forcing term associated with the Stokes drift vertical shear as well as various modifications of its boundary condition described in Sec. 2.3.

The development of a coupling infrastructure based on OASIS3-MCT has several advantages as it allows for an efficient data exchange (including the treatment of non-conformities between the computational grids) but also for versatility in the inclusion of a wave model in existing ocean-atmosphere or ocean-only models. At a practical level, the OASIS interface we have implemented in NEMO is similar to other interfaces (e.g. toward atmospheric models) existing in the code which is important for maintenance and for further developments. It paves the way for a seamless and more systematic inclusion of the coupling with waves for NEMO users.

Unlike most previous studies of wave-ocean coupling using NEMO, we have shown that satisfactory results can be obtained from the TKE vertical turbulent closure scheme without activating the *ad hoc* parameterization for the mixing induced by near-inertial waves, surface waves and ~~swells~~ swell (known as ETAU parameterization). This parameterization which amounts to empirically propagate the surface TKE at depth using a prescribed shape function is a pragmatic way to cure the shallow mixed layer depths in the southern ocean found in simulations ignoring wave effects. Previous studies of wave-ocean coupling by Breivik et al. (2015), Alari et al. (2016) or Staneva et al. (2017) have been using the ETAU parameterization in their setup. However, as suggested by Breivik et al. (2015), we can speculate that such parameterization could mask the impact of the wave coupling even though it turned out to be necessary to obtain realistic mixed layer depths. We believe that our ~~modifications~~ modification of the standard NEMO 1-equation TKE scheme described in Sec. 2.3 ~~are~~ is more physically justifiable than the ETAU parameterization and ~~require~~ requires much less parameter tuning.

The numerical experiments based on the ORCA25 configuration discussed in Sec. 4.2 were meant to check that our developments were having the expected impact on numerical solutions. First, we confirmed that using the Charnock parameter computed in the wave model instead of a constant value globally increases the wind-stress magnitude, particularly at mid and high latitudes whereas accounting for the portion of the wind-stress consumed by the waves has a small impact (in our experiments it leads to a maximum of 2% decrease of the wind-stress). Second, using the mixed layer depth as an indicator to assess the amount of vertical mixing, the modifications brought to the NEMO turbulence scheme (i.e the new boundary condition for TKE and for the mixing length, the addition of the Stokes shear in the TKE equation, and the modified Axell (2002) parameterization for Langmuir cells) lead to an important extra mixing contributing to a deepening of the surface mixed layer particularly in the southern hemisphere. When compared to ARGO data it shows a significant improvement during the summer, while during the winter the extra ~~mixing induced by waves~~ wave-induced mixing deepens the already too deep mixed layer. Note that the Fox-Kemper et al. (2008) parameterization to account for the restratification induced by mixed layer instabilities (Boccaletti et al., 2007; Couvelard et al., 2015) during the winter was not used in our experiments. This parameterization induces even more shallow summer mixed layer depths. As far as the northern hemisphere is concerned, coupled results show an improvement when compared to ARGO for winter with a deepening of the mixed layer while in summer results are similar to the uncoupled case. Since the comparison with ARGO data can be tricky due to the scarcity of the data, we looked at the results in terms of mixed layer depths (MLD) probability density functions. This allowed to highlight the significant improvement in

MLD distribution when coupling with the waves. Furthermore, we noticed that all components of the ocean-wave coupling act to deepen the mixed layer and therefore have a cumulative effect. However the main contributor is the ~~modified~~ fully modified TKE scheme including Langmuir cell parameterization of Axell (2002) which is consistent with recent results obtained by Reichl et al. (2016) and Ali et al. (2019) using a KPP closure scheme.

Since the magnitude of the vertical mixing is increased by the coupling with waves we expect an impact on sea surface temperature and currents. Indeed, the summer deepening of the mixed layer in the southern hemisphere leads to colder sea surface temperatures resulting in a better agreement with OSTIA SST analysis. More generally, although the global SST biases are not totally compensated, they tend to be reduced when considering the effect of waves (see Sec. 4.2.4). The currents in the oceanic surface boundary layer are reduced by the Stokes Coriolis force (which counteracts the Ekman current, Rascle et al., 2008). They are also affected by the increased vertical mixing which tends to reduce the surface currents (and thus the surface kinetic energy) and strengthen the currents at the base of the surface boundary layer. The reduction of surface kinetic energy due to the wave-ocean coupling in the global $1/4°$ resolution configuration is of the same order of magnitude as the reduction observed when accounting for surface currents in the computation of the wind stress in a coupled ocean-atmosphere model (e.g. Renault et al., 2016). A fully coupled ocean-wave-atmosphere model would thus be necessary to properly disentangle the different contributions at play impacting the oceanic surface kinetic energy. Even if additional diagnostics on various configurations at different resolutions are still needed to exhaustively evaluate the impact of each component of the ocean wave coupling, the results presented in the paper confirm the robustness of our developments and our implementation will serve as a starting point for the inclusion of wave-currents interactions in the forthcoming NEMO official release. We can speculate that the ocean-waves coupled ORCA025 configuration might become a standard component of future Coupled Model Intercomparison Project (CMIP) exercises. We already mentioned as a perspective the addition of a coupling with an interactive atmospheric boundary layer either via a full atmospheric model or a simplified boundary layer model (e.g. Lemarié et al., 2020). Furthermore, the gain of an online 2-way coupling compared to a 1-way coupling on the oceanic as well as on the wave solution must be investigated in the future. Indeed, the improvements of the quality of surface waves simulations associated to a coupling with large-scale oceanic currents are well documented particularly in the Agulhas current (Irvine and Tilley, 1988) and in the Gulf Stream (Mapp et al., 1985). Ardhuin et al. (2017a) have also shown a strong impact of small-scale currents (10-100km) on wave height variability at the same scales. We can therefore expect improvements for both wave and ocean forecasts when the coupling is implemented in an operational context.

Code and data availability. The changes to the NEMO code have been made on the standard NEMO code (nemo_v3_6_STABLE). The code can be downloaded from the NEMO website (http://www.nemo-ocean.eu/, last access: 11 July 2019). The NEMO code modified to include wave-ocean coupling terms and the OASIS interface is available in the zenodo archive (https://doi.org/10.5281/zenodo.3331463, Couvelard (2019)). The WW3 code version 6.02 has been used without further modifications and can be downloaded from the NOAA github repository (https://github.com/NOAA-EMC/WW3, last access: 11 July 2019). Our modifications of the OASIS interface in the WW3 code have already been integrated in the official release. The OASIS3_MCT code is also freely available (https://portal.enes.org/oasis/, last access:

11 July 2019). The exact versions of the WW3 and OASIS3_MCT codes that were used have also been made available in the zenodo archive (https://doi.org/10.5281/zenodo.3331463, Couvelard (2019)) The initial and forcing data for both the oceanic and wave model, analysis scripts, namelists and data used to produce the figures are also available in the zenodo archive.

Appendix A: Flux-form wave-averaged momentum equations

In this appendix we describe the necessary changes when a flux formulation for advective terms in the momentum equations is preferred to the vector invariant form presented in (7) and (8). For simplicity, we consider just the i-component in horizontal curvilinear coordinates and a z-coordinate in the vertical (results will be extended to the j-component and to generalized vertical coordinate). Consistently with the notations of Madec (2012), e_1 and e_2 are the horizontal scale factors. We note A_v^u the extra term needed to guarantee the equivalence between the flux formulation and the vector-invariant form. A_v^u is defined such that

$$\nabla \cdot (\mathbf{u}^s u) + \mathrm{A}_v^u = -\zeta v^s + \frac{w^s}{e_3}\partial_k u.$$

Since $\nabla \cdot \mathbf{u}^s = 0$ we have $\nabla \cdot (\mathbf{u}^s u) = \mathbf{u}^s \cdot \nabla u$, and thus

$$\begin{aligned}
\mathrm{e}_1\mathrm{e}_2\mathrm{A}_v^u &= -v^s\left[\partial_i(\mathrm{e}_2 v) - \partial_j(\mathrm{e}_1 u)\right] + \frac{\mathrm{e}_1\mathrm{e}_2}{\mathrm{e}_3} w^s \partial_k u - \left[\mathrm{e}_2 u^s \partial_i u + \mathrm{e}_1 v^s \partial_j u + \frac{\mathrm{e}_1\mathrm{e}_2}{\mathrm{e}_3} w^s \partial_k u\right] \\
&= -v^s\left[v\partial_i \mathrm{e}_2 - u\partial_j \mathrm{e}_1 + \mathrm{e}_2\partial_i v - \mathrm{e}_1 \partial_j u\right] - \mathrm{e}_2 u^s \partial_i u - \mathrm{e}_1 v^s \partial_j u
\end{aligned}$$

hence

$$\mathrm{A}_v^u = \underbrace{-\frac{v^s}{\mathrm{e}_1\mathrm{e}_2}\left(v\partial_i \mathrm{e}_2 - u\partial_j \mathrm{e}_1\right)}_{\text{Metric term on Stokes drift}} \; \underbrace{-\left(\frac{u^s}{\mathrm{e}_1}\partial_i u + \frac{v^s}{\mathrm{e}_1}\partial_i v\right)}_{\text{Additional term}}$$

Same computation for the j-component leads to the following equations in generalized vertical coordinates

$$\begin{aligned}
\frac{1}{\mathrm{e}_3}\partial_t(\mathrm{e}_3 u) &= -\frac{1}{\mathrm{e}_1\mathrm{e}_2}\left[\partial_i(\mathrm{e}_2(u+\widetilde{u}^s)u) + \partial_j(\mathrm{e}_1(v+\widetilde{v}^s)u)\right] + \frac{1}{\mathrm{e}_3}\partial_k((\omega+\widetilde{\omega}^s)u) + \left[f + \frac{1}{\mathrm{e}_1\mathrm{e}_2}\left(v\partial_i \mathrm{e}_2 - u\partial_j \mathrm{e}_1\right)\right](v+\widetilde{v}^s) \\
&+ \frac{\widetilde{u}^s}{\mathrm{e}_1}\left(\partial_i u\right)_z + \frac{\widetilde{v}^s}{\mathrm{e}_1}\left(\partial_i v\right)_z - \frac{1}{\rho_0 \mathrm{e}_1}\partial_i(p_s + \widetilde{p}^J) - \frac{1}{\rho_0 \mathrm{e}_1}\left(\partial_i p_h - \frac{(\partial_k p_h)(\partial_i z)}{\mathrm{e}_3}\right)_z + \frac{1}{\mathrm{e}_3}\partial_k\left\langle u' w \omega'\right\rangle + F^u + \widetilde{F}^u \\
\frac{1}{\mathrm{e}_3}\partial_t(\mathrm{e}_3 v) &= -\frac{1}{\mathrm{e}_1\mathrm{e}_2}\left[\partial_i(\mathrm{e}_2(u+\widetilde{u}^s)v) + \partial_j(\mathrm{e}_1(v+\widetilde{v}^s)v)\right] + \frac{1}{\mathrm{e}_3}\partial_k((\omega+\widetilde{\omega}^s)v) - \left[f + \frac{1}{\mathrm{e}_1\mathrm{e}_2}\left(v\partial_i \mathrm{e}_2 - u\partial_j \mathrm{e}_1\right)\right](u+\widetilde{u}^s) \\
&+ \frac{\widetilde{u}^s}{\mathrm{e}_2}\left(\partial_j u\right)_z + \frac{\widetilde{v}^s}{\mathrm{e}_2}\left(\partial_j v\right)_z - \frac{1}{\rho_0 \mathrm{e}_2}\partial_j(p_s + \widetilde{p}^J) - \frac{1}{\rho_0 \mathrm{e}_2}\left(\partial_j p_h - \frac{(\partial_k p_h)(\partial_j z)}{\mathrm{e}_3}\right)_z + \frac{1}{\mathrm{e}_3}\partial_k\left\langle u v' w \omega'\right\rangle + F^{uv} + \widetilde{F}^{uv}
\end{aligned}$$

where $(\partial_i \bullet)_z$ and $(\partial_j \bullet)_z$ are derivatives along z-coordinate.

Appendix B: Sensitivity to the c_{LC} parameter from single-column experiments

Single column experiments based on Noh et al. (2016) have been performed to study the behavior of the NEMO vertical closure with the Langmuir cells parameterization of Axell (2002). In the Noh et al. (2016) experiments the initial condition is given by

$$u(z,t) = v(z,t) = 0, \qquad \theta(z,t) = \min\left\{ T_0 - N_0^2 \frac{(z-5.)}{\alpha g}, T_0 \right\}$$

with α the thermal expansion coefficient in the equation of state defined as $\rho = -\alpha\rho_0(T - T_0)$ with $\rho_0 = 1024\,\mathrm{kg\,m^{-3}}$. A zonal wind is imposed with $u_\star = 0.02\,\mathrm{m\,s^{-1}}$ and the Stokes drift is given by

$$\mathbf{u}_s = (u_s, 0), \qquad u_s = \left(\frac{2\pi a}{\lambda}\right)^2 \sqrt{\frac{g\lambda}{2\pi}} e^{-4\pi z/\lambda}$$

The various parameter values are

$$f_{\mathrm{cor}} = 10^{-4}\,\mathrm{s^{-1}}, \qquad h_{\max} = 120\,\mathrm{m}, \qquad T_0 = 16\,^0\mathrm{C}, \qquad N_0^2 = 10^{-5}\,\mathrm{s^{-2}}$$

with 96 vertical levels for the discretization and 16 hours simulations. We only consider the case with $a = 1\,\mathrm{m}$ and $\lambda = 40\,\mathrm{m}$ which gives a turbulent Langmuir number of $\mathrm{La}_t \approx 0.32$. Numerical results are shown in Fig. B1 (upper panels) and are consistent with the results of Noh et al. (2016) with a deepening of the oceanic mixing length of about $10\,\mathrm{m}$ when Langmuir turbulence is accounted for ~~.~~ (see LES results in Fig. 3 in Noh et al. (2016)). For $C_{\mathrm{LC}} = 0.15$ in the Axell (2002) parameterization, the deepening is too weak while for $C_{\mathrm{LC}} = 0.3$ it is closer to Noh et al. (2016) LES results. Note that for those experiments, the value of d_{LC} is almost identical to the mixed layer depth. Fig. B1 (lower panels) illustrates the fact that for a stronger stratification (i.e. with $N_0^2 = 2\times10^{-4}\,\mathrm{s^{-2}}$ instead of $N_0^2 = 10^{-5}\,\mathrm{s^{-2}}$) the effect of Langmuir turbulence on mixed-layer depth is negligible. Indeed in this case Langmuir cells do not provide enough mixing to erode the stratification.

Author contributions. Xavier Couvelard has prepared and carried out all the numerical experiments, has investigated the results, and wrote the paper with the help of all the coauthors. Gurvan Madec, Florian Lemarié, Rachid Benshila and Xavier Couvelard have made the changes in the NEMO code to include the wave-ocean interactions. Guillaume Samson helped to prepare the necessary datasets for the numerical experiments and analyse the model outputs. Fabrice Ardhuin and Jean-Luc Redelsperger helped to investigate the results and to formalize the necessary wave-induced terms both in the primitive equations and in the TKE closure.

Competing interests. The authors declare that they have no conflict of interest.

Acknowledgements. We thank Knut Klingbeil, Patrick Marchesiello and Patrick Marsaleix for useful discussions, as well as George Nurser and Oyvind Breivik whose efforts helped to improve this paper. Xavier Couvelard, Florian Lemarié and Jean-Luc Redelsperger acknowledge the support by Mercator-Ocean and the Copernicus Marine Environment Monitoring Service (CMEMS) through contract 22-GLO-HR - Lot

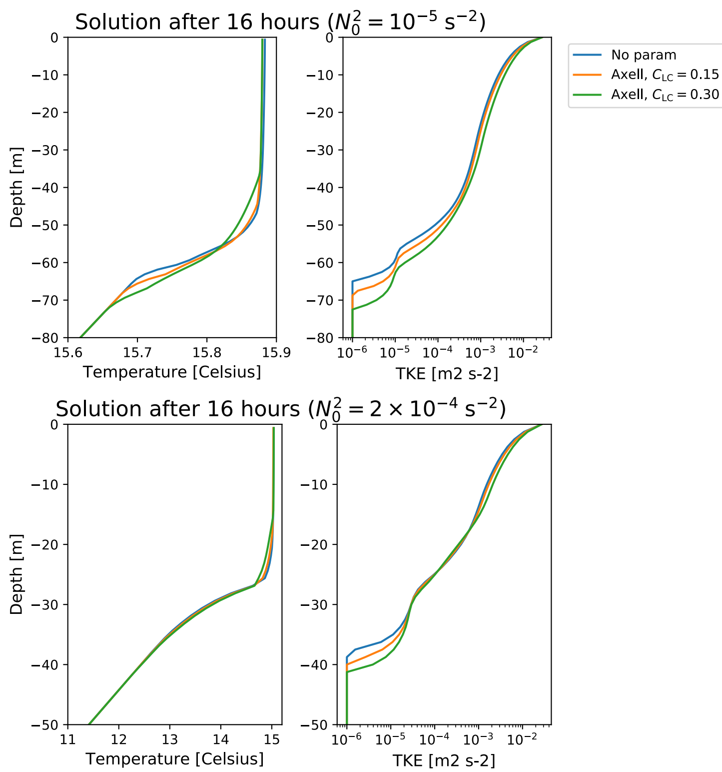

Figure B1. Solution obtained for the Noh et al. (2016) single column experiment after 16 hours for different parameter value in the Axell (2002) Langmuir cell parameterization in the case $N_0^2 = 10^{-5}\ \mathrm{s}^{-2}$ (upper panels) and $N_0^2 = 2 \times 10^{-4}\ \mathrm{s}^{-2}$ (lower panels).

2 (High-resolution ocean, waves, atmosphere interaction). Numerical simulations were performed on Ifremer HPC facilities DATARMOR of "Pôle de Calcul Intensif pour la Mer" (PCIM) (http://www.ifremer.fr/pcim). Mixed Layer Depth Data were graciously provided by Clément de Boyer Montégut, and SST data were downloaded from the CMEMS catalogue. The Authors also greatfully thanks Claude Talandier for its help with NEMO, Mickaël Accensi for its help with WW3 and Eric Maisonnave and Laure Coquart for their help with OASIS3_MCT.

References

Alari, V., Staneva, J., Breivik, Ø., Bidlot, J.-R., Mogensen, K., and Janssen, P.: Surface wave effects on water temperature in the Baltic Sea: simulation with the coupled NEMO-WAM model, Ocean Dyn., 66, 917–930, https://doi.org/10.1007/s10236-016-0963-x, 2016.

Ali, A., Christensen, K. H., Øyvind Breivik, Malila, M., Raj, R. P., Bertino, L., Chassignet, E. P., and Bakhoday-Paskyabi, M.: A comparison of Langmuir turbulence parameterizations and key wave effects in a numerical model of the North Atlantic and Arctic Oceans, Ocean Modell., https://doi.org/https://doi.org/10.1016/j.ocemod.2019.02.005, 2019.

Arakawa, A. and Lamb, V. R.: A Potential Enstrophy and Energy Conserving Scheme for the Shallow Water Equations, Mon. Weather Rev., 109, 18–36, https://doi.org/10.1175/1520-0493(1981)109<0018:APEAEC>2.0.CO;2, 1981.

Ardhuin, F. and Jenkins, A. D.: On the interaction of surface waves and upper ocean turbulence, J. Phys. Oceanogr., 36, 551–557, https://doi.org/10.1175/JPO2862.1, 2006.

Ardhuin, F., Herbers, T. H. C., Watts, K. P., van Vledder, G. P., Jensen, R., and Graber, H. C.: Swell and Slanting-Fetch Effects on Wind Wave Growth, J. Phys. Oceanogr., 37, 908–931, https://doi.org/10.1175/JPO3039.1, 2007.

Ardhuin, F., Rascle, N., and Belibassakis, K.: Explicit wave-averaged primitive equations using a generalized Lagrangian mean, Ocean Modell., 20, 35 – 60, https://doi.org/https://doi.org/10.1016/j.ocemod.2007.07.001, http://www.sciencedirect.com/science/article/pii/S1463500307000972, 2008.

Ardhuin, F., Marié, L., Rascle, N., Forget, P., and Roland, A.: Observation and estimation of Lagrangian, Stokes and Eulerian currents induced by wind and waves at the sea surface, J. Phys. Oceanogr., 39, 2820–2838, https://doi.org/10.1175/2009JPO4169.1, http://journals.ametsoc.org/doi/pdf/10.1175/2009JPO4169.1, 2009.

Ardhuin, F., Rogers, E., Babanin, A., Filipot, J.-F., Magne, R., Roland, A., van der Westhuysen, A., Queffeulou, P., Lefevre, J.-M., Aouf, L., and Collard, F.: Semi-empirical dissipation source functions for wind-wave models: part I, definition, calibration and validation, J. Phys. Oceanogr., 40, 1917–1941, https://doi.org/10.1175/2010JPO4324.1, 2010a.

Ardhuin, F., Rogers, E., Babanin, A. V., Filipot, J.-F., Magne, R., Roland, A., van der Westhuysen, A., Queffeulou, P., Lefevre, J.-M., Aouf, L., and Collard, F.: Semiempirical Dissipation Source Functions for Ocean Waves. Part I: Definition, Calibration, and Validation, J. Phys. Oceanogr., 40, 1917–1941, https://doi.org/10.1175/2010JPO4324.1, 2010b.

Ardhuin, F., Rascle, N., Chapron, B., Gula, J., Molemaker, J., Gille, S. T., Menemenlis, D., and Rocha, C.: Small scale currents have large effects on wind wave heights, J. Geophys. Res., 122, 4500–4517, https://doi.org/10.1002/2016JC012413, 2017a.

Ardhuin, F., Suzuki, N., McWilliams, J. C., and Aiki, H.: Comments on "A Combined Derivation of the Integrated and Vertically Resolved, Coupled Wave–Current Equations", J. Phys. Oceanogr., 47, 2377–2385, https://doi.org/10.1175/JPO-D-17-0065.1, 2017b.

Axell, L. B.: Wind-driven internal waves and Langmuir circulations in a numerical ocean model of the southern Baltic Sea, J. Geophys. Res., 107, 25–1–25–20, https://doi.org/10.1029/2001JC000922, http://dx.doi.org/10.1029/2001JC000922, 2002.

Banner, M. L. and Morison, R. P.: Refined source terms in wind wave models with explicit wave breaking prediction. Part I: Model framework and validation against field data, Ocean Modell., 33, 177 – 189, https://doi.org/https://doi.org/10.1016/j.ocemod.2010.01.002, http://www.sciencedirect.com/science/article/pii/S1463500310000041, 2010.

Banner, M. L. and Young, I. R.: Modeling Spectral Dissipation in the Evolution of Wind Waves. Part I: Assessment of Existing Model Performance, J. Phys. Oceanogr., 24, 1550–1571, https://doi.org/10.1175/1520-0485(1994)024<1550:MSDITE>2.0.CO;2, 1994.

Barnier, B., Madec, G., Penduff, T., Molines, J.-M., Treguier, A.-M., Le Sommer, J., Beckmann, A., Biastoch, A., Böning, C., Dengg, J., Derval, C., Durand, E., Gulev, S., Remy, E., Talandier, C., Theetten, S., Maltrud, M., McClean, J., and De Cuevas, B.: Impact of partial steps and momentum advection schemes in a global ocean circulation model at eddy-permitting resolution, Ocean Dyn., 56, 543–567, https://doi.org/10.1007/s10236-006-0082-1, https://doi.org/10.1007/s10236-006-0082-1, 2006.

Belcher, S. E., Grant, A. L. M., Hanley, K. E., Fox-Kemper, B., Van Roekel, L., Sullivan, P. P., Large, W. G., Brown, A., Hines, A., Calvert, D., Rutgersson, A., Pettersson, H., Bidlot, J.-R., Janssen, P. A. E. M., and Polton, J. A.: A global perspective on Langmuir turbulence in the ocean surface boundary layer, Geophys. Res. Lett., 39, https://doi.org/10.1029/2012GL052932, 2012.

Bennis, A.-C., Ardhuin, F., and Dumas, F.: On the coupling of wave and three-dimensional circulation models: Choice of theoretical framework, practical implementation and adiabatic tests, Ocean Modell., 40, 260 – 272, https://doi.org/https://doi.org/10.1016/j.ocemod.2011.09.003, 2011.

Boccaletti, G., Ferrari, R., and Fox-Kemper, B.: Mixed Layer Instabilities and Restratification, J. Phys. Oceanogr., 37, 2228–2250, https://doi.org/10.1175/JPO3101.1, 2007.

Boutin, G., Lique, C., Ardhuin, F., Accensi, M., Rousset, C., Talandier, C., and Girard-Ardhuin, F.: Coupling a spectral wave model with a coupled ocean-ice model, Drakkar meeting, Grenoble, France, January 21-23, http://pp.ige-grenoble.fr/pageperso/barnierb/WEBDRAKKAR2019/, 2019.

Breivik, Ø., Janssen, P., and Bidlot, J.-R.: Approximate Stokes Drift Profiles in Deep Water, J. Phys. Oceanogr., 44, 2433–2445, 2014.

Breivik, Ø., Mogensen, K., Bidlot, J.-R., Balmaseda, M. A., and Janssen, P.: Surface Wave Effects in the NEMO Ocean Model: Forced and Coupled Experiments, J. Geophys. Res., https://doi.org/10.1002/2014JC010565, 2015.

Breivik, Ø., Bidlot, J.-R., and Janssen, P.: A Stokes drift approximation based on the Phillips spectrum, Ocean Modell., 100, 49 – 56, https://doi.org/https://doi.org/10.1016/j.ocemod.2016.01.005, 2016.

Brodeau, L., Barnier, B., Gulev, S. K., and Woods, C.: Climatologically significant effects of some approximations in the bulk parameterizations of turbulent air-sea fluxes, J. Phys. Oceanogr., 0, null, https://doi.org/10.1175/JPO-D-16-0169.1, 2016.

Charnock, H.: Wind stress on a water surface, Quart. J. Roy. Meteorol. Soc., 81, 639–640, https://doi.org/10.1002/qj.49708135027, https://rmets.onlinelibrary.wiley.com/doi/abs/10.1002/qj.49708135027, 1955.

Chen, G. and Belcher, S. E.: Effects of Long Waves on Wind-Generated Waves, J. Phys. Oceanogr., 30, 2246–2256, 2000.

Chen, Shuyi, S. and Curnic, M.: Ocean surface waves in Hurricane Ike (2008) and Superstorm Sandy (2012): Coupled model predictions and observations, Oceanogr. Meteorol., 103, 161–176, https://doi.org/10.5670/oceanog.2010.05, 2015.

Couvelard, X.: ORCA025-WW3-Couvelard_etal_GMD, https://doi.org/10.5281/zenodo.3331463, https://doi.org/10.5281/zenodo.3331463, 2019.

Couvelard, X., Dumas, F., Garnier, V., Ponte, A., Talandier, C., and Treguier, A.: Mixed layer formation and restratification in presence of mesoscale and submesoscale turbulence, Ocean Modell., 96, 243 – 253, https://doi.org/https://doi.org/10.1016/j.ocemod.2015.10.004, 2015.

Craig, A., Valcke, S., and Coquart, L.: Development and performance of a new version of the OASIS coupler, OASISMCT3.0, Geosci. Model Dev., 10, 3297–3308, https://doi.org/10.5194/gmd-10-3297-2017, 2017.

Craig, P. D. and Banner, M. L.: Modeling Wave-Enhanced Turbulence in the Ocean Surface Layer, J. Phys. Oceanogr., 24, 2546–2559, 1994.

D'Asaro, E. A., Thomson, J., Shcherbina, A. Y., Harcourt, R. R., Cronin, M. F., Hemer, M. A., and Fox-Kemper, B.: Quantifying upper ocean turbulence driven by surface waves, Geophys. Res. Lett., 41, 102–107, https://doi.org/10.1002/2013GL058193, https://agupubs.onlinelibrary.wiley.com/doi/abs/10.1002/2013GL058193, 2014.

de Boyer Montégut, C., Madec, G., Fischer, A. S., Lazar, A., and Iudicone, D.: Mixed layer depth over the global ocean: An examination of profile data and a profile-based climatology, J. Geophys. Res., 108, https://doi.org/10.1029/2004JC002378, 2004.

Deardorff, J. W.: Stratocumulus-capped mixing layers derived from a threedimensional model, Boundary-Layer Meteorol., 18, 495–527, 1980.

Dee, D. P., Uppala, S. M., Simmons, A. J., Berrisford, P., Poli, P., Kobayashi, S., Andrae, U., Balmaseda, M. A., Balsamo, G., Bauer, P., Bechtold, P., Beljaars, A. C. M., van de Berg, L., Bidlot, J., Bormann, N., Delsol, C., Dragani, R., Fuentes, M., Geer, A. J., Haimberger, L., Healy, S. B., Hersbach, H., Hólm, E. V., Isaksen, L., Kållberg, P., Köhler, M., Matricardi, M., McNally, A. P., Monge-Sanz, B. M., Morcrette, J.-J., Park, B.-K., Peubey, C., de Rosnay, P., Tavolato, C., Thépaut, J.-N., and Vitart, F.: The ERA-Interim reanalysis: configuration and performance of the data assimilation system, Quarterly Journal of the Royal Meteorological Society, 137, 553–597, https://doi.org/10.1002/qj.828, https://rmets.onlinelibrary.wiley.com/doi/abs/10.1002/qj.828, 2011.

Ducousso, N., Le Sommer, J., Molines, J.-M., and Bell, M.: Impact of the "Symmetric Instability of the Computational Kind" at mesoscale- and submesoscale-permitting resolutions, Ocean Modell., 120, 18–26, https://doi.org/10.1016/j.ocemod.2017.10.006, 2017.

Fairall, C. W., Bradley, E. F., Hare, J. E., Grachev, A. A., and Edson, J. B.: Bulk Parameterization of Air–Sea Fluxes: Updates and Verification for the COARE Algorithm, J. Climate, 16, 571–591, https://doi.org/10.1175/1520-0442(2003)016<0571:BPOASF>2.0.CO;2, 2003.

Fan, Y. and Griffies, S. M.: Impacts of Parameterized Langmuir Turbulence and Nonbreaking Wave Mixing in Global Climate Simulations, J. Climate, 27, 4752–4775, https://doi.org/10.1175/JCLI-D-13-00583.1, 2014.

Fox-Kemper, B., Ferrari, R., and Hallberg, R.: Parameterization of Mixed Layer Eddies. Part I: Theory and Diagnosis, Journal of Physical Oceanography, 38, 1145–1165, https://doi.org/10.1175/2007JPO3792.1, 2008.

Hasselmann, K.: Ocean circulation and climate change, Tellus B: Chemical and Physical Meteorology, 43, 82–103, https://doi.org/10.3402/tellusb.v43i4.15399, https://doi.org/10.3402/tellusb.v43i4.15399, 1991.

Hasselmann, S., Hasselmann, K., Allender, H., and Barnet, T. P.: Computations and parameterizations of the nonlinear energy transfer in a gravity wave spectrum. Part II. Parameterizations of the nonlinear energy transfer for application in wave models , J. Phys. Oceanogr., 15, 1378–1391, 1985.

Hilburn, K.: The passive microwave water cycle product, Remote Sensing Systems (REMSS) Technical Report 072409, Santa Rosa (CA), 30pp , Tech. rep., 2009.

Hwang, P. A.: Fetch- and Duration-Limited Nature of Surface Wave Growth inside Tropical Cyclones: With Applications to Air–Sea Exchange and Remote Sensing*, J. Phys. Oceanogr., 46, 41–56, 2015.

Irvine, D. E. and Tilley, D. G.: Ocean wave directional spectra and wave-current interaction in the Agulhas from the Shuttle Imaging Radar-B synthetic aperture radar, Journal of Geophysical Research: Oceans, 93, 15 389–15 401, https://doi.org/10.1029/JC093iC12p15389, https://agupubs.onlinelibrary.wiley.com/doi/abs/10.1029/JC093iC12p15389, 1988.

Jacob, R., Larson, J., and Ong, E.: M × N Communication and Parallel Interpolation in Community Climate System Model Version 3 Using the Model Coupling Toolkit, The International Journal of High Performance Computing Applications, 19, 293–307, https://doi.org/10.1177/1094342005056116, https://doi.org/10.1177/1094342005056116, 2005.

Janssen, P. A.: Progress in ocean wave forecasting, J. Comp. Phys., 227, 3572 – 3594, https://doi.org/https://doi.org/10.1016/j.jcp.2007.04.029, http://www.sciencedirect.com/science/article/pii/S0021999107001659, predicting weather, climate and extreme events, 2008.

Janssen, P. A. E. M.: Quasi-linear Theory of Wind-Wave Generation Applied to Wave Forecasting, J. Phys. Oceanogr., 21, 1631–1642, 1991.

Janssen, P. A. E. M.: On some consequences of the canonical transformation in the Hamiltonian theory of water waves, JOURNAL OF FLUID MECHANICS, 637, 1–44, https://doi.org/10.1017/S0022112009008131, 2009.

Komen, G. J., Cavaleri, L., Donelan, M., Hasselmann, K., Hasselmann, S., and Janssen, P. A. E. M.: Dynamics and modelling of ocean waves, Cambridge University Press, Cambridge, 1994.

Large, W. G. and Yeager, S. G.: The global climatology of an interannually varying air–sea flux data set, Clim. Dyn., 33, 341–364, https://doi.org/10.1007/s00382-008-0441-3, 2009.

Law Chune, S. and Aouf, L.: Wave effects in global ocean modeling: parametrizations vs. forcing from a wave model, Ocean Dyn., 68, 1739–1758, https://doi.org/10.1007/s10236-018-1220-2, 2018.

Leclair, M. and Madec, G.: A conservative leap-frog time stepping method, Oceanogr. Meteorol., 30, 88–94, https://doi.org/10.1016/j.ocemod.2009.06.006, 2009.

Lemarié, F., Samson, G., Redelsperger, J.-L., Giordani, H., Brivoal, T., Masson, S., and Madec, G.: A simplified atmospheric boundary layer model for an improvedrepresentation of air-sea interactions in eddying oceanic models:implementation and first evaluation in NEMO(4.0), Geosci. Model Dev., in preparation, 2020.

Li, Q., Webb, A., Fox-Kemper, B., Craig, A., and Danabasoglu, G.: Langmuir mixing effects on global climate: WAVEWATCH III in CESM, Oceanogr. Meteorol., 103, 145–160, https://doi.org/10.1016/j.ocemod.2015.07.020, 2016.

Li, Q., Fox-Kemper, B., Breivik, O., and Webb, A.: Statistical models of global Langmuir mixing, Oceanogr. Meteorol., 113, 95–114, https://doi.org/10.1016/j.ocemod.2017.03.016, 2017.

Lévy, M., Estublier, A., and Madec, G.: Choice of an advection scheme for biogeochemical models, Geophys. Res. Lett., 28, 3725–3728, https://doi.org/10.1029/2001GL012947, 2001.

Madec, G.: NEMO ocean engine, in: Note du Pole de modélisation No. 27, Institut Pierre-Simon Laplace (IPSL), France, 2012.

Mapp, G. R., Welch, C. S., and Munday, J. C.: Wave refraction by warm core rings, Journal of Geophysical Research: Oceans, 90, 7153–7162, https://doi.org/10.1029/JC090iC04p07153, https://agupubs.onlinelibrary.wiley.com/doi/abs/10.1029/JC090iC04p07153, 1985.

McWilliams, J. C., Restrepo, J. M., and Lane, E. M.: An asymptotic theory for the interaction of waves and currents in coastal waters, J. Fluid Mech., 511, 135–178, https://doi.org/10.1017/S0022112004009358, 2004.

Mellor, G. and Blumberg, A.: Wave breaking and ocean surface layer thermal response, J. Phys. Oceanogr., 34, 693–698, 2004.

Michaud, H., Marsaleix, P., Leredde, Y., Estournel, C., Bourrin, F., Lyard, F., Mayet, C., and Ardhuin, F.: Three-dimensional modelling of wave-induced current from the surf zone to the inner shelf, Ocean Sci., 8, 657–681, https://doi.org/10.5194/os-8-657-2012, 2012.

Moghimi, S., Klingbeil, K., Gräwe, U., and Burchard, H.: A direct comparison of a depth-dependent Radiation stress formulation and a Vortex force formulation within a three-dimensional coastal ocean model, Ocean Modell., 70, 132 – 144, https://doi.org/https://doi.org/10.1016/j.ocemod.2012.10.002, http://www.sciencedirect.com/science/article/pii/S1463500312001473, ocean Surface Waves, 2013.

Noh, Y., Ok, H., Lee, E., Toyoda, T., and Hirose, N.: Parameterization of Langmuir Circulation in the Ocean Mixed Layer Model Using LES and Its Application to the OGCM, J. Phys. Oceanogr., 46, 57–78, 2016.

Phillips, O.: On the response of short ocean wave components at fixed wavenumber to ocean current variations, J. Phys. Oceanogr., 14, 1425–1433, 1984.

Polonichko, V.: Generation of Langmuir circulation for nonaligned wind stress and the Stokes drift, J. Geophys. Res., 102, 15 773–15 780, https://doi.org/10.1029/97JC00460, https://agupubs.onlinelibrary.wiley.com/doi/abs/10.1029/97JC00460, 1997.

Rascle, N. and Ardhuin, F.: Drift and mixing under the ocean surface revisited: Stratified conditions and model-data comparisons, J. Geophys. Res., 114, doi:10.1029/2007JC004466, 2009.

Rascle, N. and Ardhuin, F.: A global wave parameter database for geophysical applications. Part 2: model validation with improved source term parameterization, Ocean Modelling, 70, 174–188, https://doi.org/10.1016/j.ocemod.2012.12.001, 2013.

Rascle, N., Ardhuin, F., Queffeulou, P., and Croizé-Fillon, D.: A global wave parameter database for geophysical applications. Part 1: wave-current-turbulence interaction parameters for the open ocean based on traditional parameterizations, Ocean Modell., 25, 154–171, http://hal.archives-ouvertes.fr/hal-00201380/, doi:10.1016/j.ocemod.2008.07.006, 2008.

Redelsperger, J. L., Mahé, F., and Carlotti, P.: A Simple And General Subgrid Model Suitable Both For Surface Layer And Free-Stream Turbulence, Boundary-Layer Meteorol., 101, 375–408, 2001.

Reichl, B. G., Ginis, I., Hara, T., Thomas, B., Kukulka, T., and Wang, D.: Impact of Sea-State-Dependent Langmuir Turbulence on the Ocean Response to a Tropical Cyclone, Monthly Weather Review, 144, 4569–4590, https://doi.org/10.1175/MWR-D-16-0074.1, 2016.

Renault, L., Molemaker, M. J., McWilliams, J. C., Shchepetkin, A. F., Lemarié, F., Chelton, D., Illig, S., and Hall, A.: Modulation of Wind Work by Oceanic Current Interaction with the Atmosphere, J. Phys. Oceanogr., 46, 1685–1704, https://doi.org/10.1175/JPO-D-15-0232.1, 2016.

Rodgers, K. B., Aumont, O., Mikaloff Fletcher, S. E., Plancherel, Y., Bopp, L., de Boyer Montégut, C., Iudicone, D., Keeling, R. F., Madec, G., and Wanninkhof, R.: Strong sensitivity of Southern Ocean carbon uptake and nutrient cycling to wind stirring, Biogeosciences, 11, 4077–4098, https://doi.org/10.5194/bg-11-4077-2014, https://www.biogeosciences.net/11/4077/2014/, 2014.

Roquet, F., Madec, G., McDougall, T., and Barker, P.: An accurate polynomial expression for the TEOS-10 equation of state for use in ocean general circulation models., Oceanogr. Meteorol., 90, 29–43, https://doi.org/10.1016/j.ocemod.2015.04.002, 2015.

Rousset, C., Vancoppenolle, M., Madec, G., Fichefet, T., Flavoni, S., Barthélemy, A., Benshila, R., Chanut, J., Levy, C., Masson, S., and Vivier, F.: The Louvain-La-Neuve sea ice model LIM3.6: global and regional capabilities, Geoscientific Model Development, 8, 2991–3005, https://doi.org/10.5194/gmd-8-2991-2015, https://www.geosci-model-dev.net/8/2991/2015/, 2015.

Skyllingstad, E. D. and Denbo, D. W.: An ocean large-eddy simulation of Langmuir circulations and convection in the surface mixed layer, J. Geophys. Res., 100, 8501–8522, https://doi.org/10.1029/94JC03202, 1995.

Staneva, J., Alari, V., Breivik, Ø., Bidlot, J.-R., and Mogensen, K.: Effects of wave-induced forcing on a circulation model of the North Sea, Ocean Dynamics, 67, 81–101, 2017.

Stopa, J. E., Sutherland, P., and Ardhuin, F.: Strong and highly variable push of ocean waves on Southern Ocean sea ice, Proc. Nat. Acad. Sci., 115, 5861–5865, https://doi.org/10.1073/pnas.1802011115, 2018.

Suzuki, N. and Fox-Kemper, B.: Understanding Stokes forces in the wave-averaged equations, J. Geophys. Res., 121, 3579–3596, https://doi.org/10.1002/2015JC011566, https://agupubs.onlinelibrary.wiley.com/doi/abs/10.1002/2015JC011566, 2016.

Tennekes, H. and Lumley, J. L.: A first course in turbulence, The MIT Press, 1972.

The WAVEWATCH III® Development Group: User manual and system documentation of WAVEWATCH III® version 5.16, Tech. Note 329, NOAA/NWS/NCEP/MMAB, College Park, MD, USA, 326 pp. + Appendices, 2016.

Tolman, H. L., Balasubramaniyan, B., Burroughs, L. D., Chalikov, D. V., Chao, Y. Y., Chen, H. S., and Gerald, V. M.: Development and Implementation of Wind-Generated Ocean Surface Wave Modelsat NCEP, Wea Forecasting, 17, 311–333, https://doi.org/10.1175/1520-0434(2002)017<0311:DAIOWG>2.0.CO;2, 2002.

Uchiyama, Y., McWilliams, J. C., and Shchepetkin, A. F.: Wave–current interaction in an oceanic circulation model with a vortex-force formalism: Application to the surf zone, Ocean Modell., 34, 16 – 35, https://doi.org/https://doi.org/10.1016/j.ocemod.2010.04.002, http://www.sciencedirect.com/science/article/pii/S1463500310000594, 2010.

UNESCO: Algorithms for computation of fundamental property of sea water, 44, 1983.

Valcke, S.: The OASIS3 coupler: a European climate modelling community software, Geoscientific Model Development Discussions, 5, 2139–2178, https://doi.org/10.5194/gmdd-5-2139-2012, 2012.

Van Roekel, L. P., Fox-Kemper, B., Sullivan, P. P., Hamlington, P. E., and Haney, S. R.: The form and orientation of Langmuir cells for misaligned winds and waves, J. Geophys. Res., 117, https://doi.org/10.1029/2011JC007516, https://agupubs.onlinelibrary.wiley.com/doi/abs/10.1029/2011JC007516, 2012.

Wu, L., Staneva, J., Breivik, O., Rutgersson, A., Nurser, A. G., Clementi, E., and Madec, G.: Wave effects on coastal upwelling and water level, Ocean Modell., 140, 101 405, https://doi.org/https://doi.org/10.1016/j.ocemod.2019.101405, http://www.sciencedirect.com/science/article/pii/S1463500318301409, 2019.